

THE FAR-ULTRAVIOLET SPECTRA OF EARLY-TYPE GALAXIES^{1,2}

DAVID BURSTEIN

Department of Physics, Arizona State University

F. BERTOLA

Department of Astronomy, University of Padova, Italy

L. M. BUSON

Astronomical Observatory, Padova, Italy

S. M. FABER

Lick Observatory, University of California, Santa Cruz

AND

TOD R. LAUER

Princeton University Observatory

Received 1987 July 20; accepted 1987 November 5

ABSTRACT

New and revised ultraviolet energy distributions are presented based on 97 *IUE* spectra of 31 early-type galaxies and the bulge of M31. Measurements of the line strength index Mg_2 and the V magnitude flux within the *IUE* aperture are included. The average flux between 1250 and 1850 Å is combined with the V magnitude to form an ultraviolet/optical (1550 – V) color.

Based on optical spectra and morphology, the sample galaxies are divided into three categories: four objects with abnormally high numbers of young stars (star-forming galaxies); four objects with strong, broad nuclear emission lines (active galaxies); and 24 normal objects showing no clear spectral or morphological peculiarities (quiescent galaxies).

The major finding of this study is a well-defined, nonlinear relationship between (1550 – V) color and Mg_2 for the 24 quiescent galaxies. This trend is in the sense suggested by Faber in 1983: (1550 – V) color is *bluer* at higher line strength, opposite to the behavior of every other known color. Correlations of (1550 – V) color with velocity dispersion and total luminosity have also been tested, but both are weaker. In comparison to the quiescent galaxies the four star-forming galaxies clearly show excess UV flux due to the impact of young stars. The four active galaxies with nuclear emission also show a UV excess, but of much smaller magnitude.

The ultraviolet spectra of quiescent galaxies can be modeled as a sum of two components: a normal, cool stellar population of main-sequence and giant branch stars that is redder at higher Mg_2 (in the normal sense), plus a very blue population having a steeply rising UV flux below 2000 Å that increases in strength with metallicity. This blue component affects the whole spectrum shortward of 3200 Å, and its much higher amplitude in high- Mg_2 galaxies is what accounts for their very blue (1500 – V) colors and relatively blue fluxes from 2600 to 3200 Å.

The ultraviolet spectra of the star-forming galaxies are significantly flatter than the very blue component of quiescent galaxies and are consistent with aging bursts of star formation. The two bluest active galaxies, N4486 and N6166, may have excess light at wavelengths between 2000 and 2500 Å compared to quiescent galaxies with similar (1500 – V) colors.

Two sample population models are explored for the blue stellar component of quiescent galaxies: post-asymptotic giant branch (PAGB) stars and young stars from continuing star formation. Although both models exhibit similar UV energy distributions which approximate the UV spectra of quiescent and active galaxies, there currently exists no satisfactory theoretical explanation of the increase of UV flux with increasing metallicity. Resolution of the origin of the far-UV flux in ellipticals can be tested both with detailed UV imaging and with very accurate spectral energy distributions of galaxies. This is an important problem for the Hubble Space Telescope.

Subject headings: galaxies: evolution — galaxies: stellar content — ultraviolet: spectra

I. INTRODUCTION

Previous ultraviolet observations of elliptical galaxies have shown that these apparently old stellar systems contain an extended stellar population that emits increasing flux with

¹ Based on observations obtained with the *International Ultraviolet Explorer Satellite*, which is sponsored and operated by the United States National Aeronautics and Space Administration, by the Science Research Council of the United Kingdom, and by the European Space Agency.

² *Lick Observatory Bulletin* No. 1096.

decreasing wavelength below 2000 Å (e.g., Code and Welch 1979; Bertola *et al.* 1980; Oke, Bertola, and Capaccioli 1981; Bertola, Capaccioli, and Oke 1982; O'Connell, Thuan, and Puschell 1986; Bertola *et al.* 1986). The level of this flux relative to visual light varies by almost an order of magnitude. Interpreting the origin of this "rising branch" of ultraviolet light has centered on one critical question: Is the emission correlated with any other dynamical or stellar population property of these galaxies, or is it a random, stochastic property?

Competing hypotheses for the origin of the ultraviolet light have been summarized by Nesci and Perola (1985) and Renzini and Buzzoni (1986). They can be broken down into four basic categories: (1) post-asymptotic giant branch stars going through the planetary nucleus stage (PAGB); (2) hot young stars that are part of a minority star-forming population; (3) a hot horizontal branch, either with or without an associated minority metal-poor population; and (4) an unusual hot stage of stellar evolution that is overabundant in the old stellar populations of ellipticals, such as accretion disks around white dwarf stars in binary star systems.

Several years ago Faber (1983) suggested a possible systematic correlation between the ultraviolet flux level of elliptical galaxies and the strength of the Mg_2 absorption line feature, in the sense that UV color is bluer at higher line strength. This trend is surprisingly opposite to the well-known color-line strength trends in the optical and near-infrared portions of the spectrum.

A possible Mg_2 -UV color relationship holds out the hope that the UV emission from ellipticals is systematic in behavior and can be understood by studying a larger sample of galaxies. Previous attempts to interpret the UV flux of elliptical galaxies had been limited to comparisons of at most three or four galaxies. This paper presents the analysis of a substantially larger sample, consisting of *IUE* observations of 31 elliptical and S0 galaxies plus the bulge of M31. Many of the *IUE* data are taken from the *IUE* archives, but nine new galaxies have also been added. All of the galaxies have short-wavelength UV spectra from 1250 to 1900 Å, and 22 also have long-wavelength spectra from 1950 to 3200 Å.

All spectra have been rereduced in a homogeneous manner using recent *IUE* calibrations as described in § II. Various global measures of the structure and stellar populations of the galaxies are also given there, as well as accurate *V* magnitudes interpolated to the effective *IUE* aperture. Section III presents the UV color- Mg_2 diagram that results from the new data, plus the correlation of UV color with central velocity dispersion.

The core of the paper is § IV, which analyzes the spectra of the 24 normal galaxies that lack strong nuclear emission or obvious star formation. Two model hot populations are presented and discussed. Four active galaxies with strong nuclear emission and small UV excesses are discussed in § V. Several theories for the UV emission of the normal and active galaxies are discussed in § VI, with special reference to the X-ray emission. The UV spectra of four galaxies undergoing obvious star formation differ strongly from all other objects and are discussed in the Appendix. Readers not interested in the observational details should skip to § III.

II. OBSERVATIONS AND DATA

a) Sample Selection

To be included in this survey a galaxy (1) must be classified as either elliptical or S0 (except for M31); (2) must have a low-resolution, short-wavelength (SW) *IUE* spectrum of reasonable integration time (typically ≥ 4 hr); and (3) must have a measured Mg_2 index on the system of Faber, Burstein, and collaborators (Faber *et al.* 1985). The sample was assembled in two stages. First, Mg_2 indices for 300 E and S0 galaxies were searched to identify the brightest galaxies with extreme values of Mg_2 , either large or small. Short-wavelength *IUE* spectra (SWP) were obtained for 10 of these galaxies during the period

1984 June–1986 October. Second, the merged *IUE* log was searched for additional SWP exposures of all early-type galaxies with measured Mg_2 . A total of 56 SWP spectra for 31 E and S0 galaxies plus the nucleus of M31 are included in this study, and inclusion of a galaxy in the sample was independent of the signal-to-noise of the SWP spectra. The merged *IUE* log was then searched for deep low-resolution LWP or LWR spectra to combine with the SWP data. Data in both wavelength regions are available for 22 galaxies, using a total of 41 LWP or LWR spectra. Many galaxies have multiple observations.

b) The *IUE* Spectra

Galaxies, Hubble types, *IUE* image numbers, exposure times, position angles and estimates of signal-to-noise ratios (*S/N*) are given in Table 1. To assure homogeneity, all spectra (both SW and LW) were rereduced by one of us (L. H. B.) in a consistent manner using the Image Handling and Processing (IHAP) software package. IHAP is a general purpose *IUE* data reduction package, and the current version was kindly provided by the European Southern Observatory.

The so-called line-by-line images (File 3 on the new standard *IUE* data tape) were used to extract the UV fluxes. These images are comprised of 55 spatially resolved gross (i.e., background + galaxy) spectra that have been extracted from the geometrically and photometrically corrected *IUE* image. The wavelength calibration was applied as part of the standard *IUE* reduction.

The following steps were taken in deriving final spectra.

1. The line-by-line spectrum was displayed in order to measure the extension of the galaxy emission in the direction perpendicular to the dispersion and to identify possible flaws in the picture (cosmic-ray events, reseau marks, etc.).

2. All lines, including several lines of background on either side, were individually displayed in order to remove the previously identified blemishes.

3. The lines of the background and lines of gross spectrum were separately co-added. The background was smoothed to a resolution of 41 pixels (approximately 100 Å) and then subtracted from the gross spectrum to produce a net raw spectrum.

4. The final spectrum was derived by applying the characteristic calibration curve of the camera (SWP, LWP, or LWR) to the net spectrum and dividing by the exposure time.

5. The results were checked by comparing the final spectrum with the results provided by the *IUE* standard extraction, yielding satisfactory agreement.

The number of lines in each *IUE* image used for the final spectra is given in Table 1. Although the *IUE* apertures project to a size of approximately 11 pixels (1 pixel = 2"1 in angular extent), diffusion effects for well-exposed images increase the effective size over which signal can be obtained to 14 lines.

As the signal-to-noise ratio per resolution element is generally low, the data are best displayed as average fluxes in 50 Å intervals. We have centered these intervals at 1250 Å, 1300 Å, ..., 3300 Å in the laboratory frame. Fluxes are given in Table 2A for the SWP spectra and in Table 2B for the LWR or LWP spectra when available. The errors in these fluxes are discussed in detail in § II*f*. Differences in effective aperture size between SW and LW exposures are discussed in the next section.

The reader should note that there are significant differences between the present spectra and previously published spectra

TABLE 1
OBSERVING PARAMETERS FOR LOW-DISPERSION *IUE* SPECTRA

Object (1)	Type (2)	Image Number (3)	P.A. (4)	Effective Aperture Width (pixels) (5)	Exposure Time (minutes) (6)	S/N (7)
NGC 205	E	SWP 10314	64°	12	420	3.9
		LWR 16363	137	12	409	4.5
		LWR 17109	175	11	270	1.4
NGC 221 (= M32)	E	SWP 3545	161	11	300	2.1
		SWP 24974	131	9	80	0.8
		SWP 24993	129	14	100	0.8
		SWP 29390	71	11	285	1.8
		LWR 4644	74	11	180	6.0
		LWR 4645	74	13	150	5.2
		LWR 8413	154	12	180	6.1
NGC 224 (= M31)	Sb	SWP 3520	164	12	481	5.4
		SWP 7376	157	14	600	4.8
		SWP 9502	139	12	430	5.4
		SWP 9519	138	14	440	5.7
		LWR 3088	166	13	298	5.2
		LWR 4682	163	14	150	4.4
		LWR 6343	159	12	340	4.7
		LWR 6368	157	12	280	5.0
		LWR 8236	138	13	441	5.9
NGC 584	E	SWP 24973	146	9	295	0.9
NGC 1052	E	SWP 3645	127	7	183	1.3
		SWP 24581	114	9	380	1.4
		LWR 3198	127	10	225	2.1
NGC 1399	E	SWP 23271	104	11	395	6.8
		SWP 28507	105	13	605	5.7
NGC 1404	E	SWP 9189	92	11	391	2.5
		LWR 7958	93	10	405	3.3
NGC 1407	E	SWP 24715	112	10	100	0.7
		SWP 25000	142	12	125	0.7
		SWP 25001	142	10	92	0.3
		SWP 29367	7	13	520	2.0
NGC 2681	Sa	SWP 15904	130	12	400	2.1
		LWR 12223	132	9	200	4.1
		LWR 12230	130	11	200	4.3
NGC 2768	E	SWP 24992	83	11	695	0.6
NGC 2784	S0	SWP 18471	174	8	331	0.8
NGC 3115	S0	SWP 10673	4	12	310	2.5
		LWR 7488	168	13	410	3.9
		LWR 9383	4	11	246	3.1
		LWR 15447	131	12	172	3.9
NGC 3379	E	SWP 5690	2	9	480	1.7
		LWR 2960	6	10	425	3.7
		LWR 4948	2	12	395	3.2
NGC 4111	S0	SWP 16659	65	11	404	1.1
NGC 4125	E	SWP 14531	146	10	413	0.9
		LWR 13025	52	12	420	2.2
NGC 4278	E	SWP 14467	175	11	406	2.4
		LWR 11055	176	12	421	3.6
NGC 4374 (= M84)	E	SWP 7895	172	12	430	1.5
		LWR 4777	8	11	400	2.7
NGC 4382 (= M85)	S0	SWP 10698	16	14	410	0.6
		LWR 9381	16	13	300	4.0
NGC 4406 (= M86)	E	SWP 7405	10	13	420	0.9
		LWR 6399	10	12	405	2.7
NGC 4472 (= M49)	E	SWP 5324	14	13	410	2.2
		SWP 7350	9	10	320	2.3
		SWP 7913	176	14	340	1.9
		SWP 7949	173	10	320	2.3
		LWR 4520	16	11	180	3.3
		LWR 4664	11	12	361	3.2
		LWR 4681	10	11	270	3.0
		LWR 6877	176	12	360	3.6
		LWR 6912	175	12	330	3.6

FAR-UV SPECTRA OF EARLY-TYPE GALAXIES

TABLE 1—Continued
OBSERVING PARAMETERS FOR LOW-DISPERSION *IUE* SPECTRA

Object (1)	Type ^a (2)	Image Number (3)	P.A. ^b (4)	Effective Aperture Width (pixels) (5)	Exposure Time (minutes) (6)	S/N ^c (7)
NGC 4486 (= M87)	E	SWP 1854	6	11	300	3.4
		SWP 4299	166	10	430	4.6
		SWP 2157	155	14	400	3.5
		LWR 3818	164	12	230	3.3
		LWR 10333	42	12	60	1.3
NGC 4494	E	SWP 24719	8	9	250	0.6
NGC 4552 (= M89)	E	SWP 19114	177	11	307	3.1
		SWP 19130	176	9	270	3.5
		SWP 22255	170	9	411	4.0
		LWR 13617	4	12	375	4.2
NGC 4621 (= M59)	E	LWR 13622	4	11	370	4.2
		SWP 24999	177	11	300	1.7
NGC 4649 (= M60)	E	LWP 8129	27	14	353	3.7
		SWP 7912	173	14	420	4.6
NGC 4697	E	SWP 8871	28	12	387	4.8
		LWR 4770	11	11	415	4.1
		LWR 7651	28	12	415	4.7
NGC 4742	E	SWP 23275	6	9	120	0.7
		SWP 24706	6	12	424	1.6
NGC 4762	S0	SWP 23274	1	9	260	2.1
		SWP 24714	5	11	700	2.9
NGC 4762	S0	SWP 13892	27	7	391	1.0
		LWR 2987	19	12	180	1.8
NGC 4889	E	LWR 19748	57	9	387	0.9
		LWP 1524	59	8	368	1.9
NGC 5102	S0	SWP 13788	99	8	252	10.0
		SWP 15886	175	10	400	15.8
		SWP 16417	23	12	360	11.4
		SWP 19055	9	9	210	8.3
		LWR 10429	101	12	340	8.7
NGC 5846	E	LWR 12239	177	11	180	7.4
		SWP 19607	153	11	381	0.8
NGC 6166	E	SWP 15520	89	10	816	0.6
		LWP 1372	89	10	792	1.3

COL. (2).—Hubble type, from RC2.

COL. (4).—Position angle of *IUE* aperture.

COL. (5).—Effective aperture size = number of lines used from *IUE* image.

COL. (7).—Averaged ratio of (smoothed spectrum)/(smoothed absolute noise). Smoothed absolute noise = (original spectrum) - (smoothed spectrum). Regions sampled: 1350–1850 Å (SW) and 1950–3200 Å (LW).

for certain galaxies (e.g., NGC 221 [=M32; Bertola *et al.* 1980] and NGC 4486 [=M87; Oke, Bertola and Capaccioli 1981]). This is due either to a revision in the standard *IUE* reduction procedure since the original spectrum was published or to the addition of two or more *IUE* spectra here.

For comparison with other parameters, a mean short-wavelength *IUE* flux is defined by averaging the flux between 1250 and 1850 Å. This average is combined with the *V* magnitude through the *IUE* aperture (defined below) to form a color (1550 - *V*), which is expressed as a magnitude. The *V* band zero point is $\log f_{V=10} = -12.41 \text{ ergs cm}^{-2} \text{ s}^{-1} \text{ Å}^{-1}$ from Johnson (1966).

c) Visual Magnitudes

Previous discussions of *IUE* spectra have shown the value of comparing well-defined ultraviolet and visual fluxes. For this

survey we have taken the standard *V* magnitude as our measure of visual flux and have derived *V* magnitudes that are consistent with the *IUE* data in the following manner.

Accurate surface photometry in the *R* band for 14 of the 32 galaxies has been obtained by Lauer (1985). The *R* band flux through the actual *IUE* aperture was compared to that through a series of circular apertures. Galaxies with a range of average ellipticity from 0.0 to 0.5 were sampled. The resulting calibration indicated that the flux through a circular aperture with a diameter of 14" is an excellent match to the flux through the full *IUE* aperture, with only a small dependence of diameter (± 0.4) or flux (± 0.02 dex) on the ellipticity of the galaxy. This test is in good agreement with previous estimates of equivalent *IUE* circular apertures (Oke, Bertola, and Capaccioli 1981).

As given in Table 1, the actual extent of each image varied

TABLE 2A
 IUE SHORT-WAVELENGTH SPECTRA, COVERING 1250 Å–1900 Å

Object	1250	1300	1350	1400	1450	1500	1550	1600	1650	1700	1750	1800	1850	1900
N205	429	491	441	432	450	466	436	360	349	502	561	487	445	418
N221	247	276	279	229	399	553	437	179	236	299	385	327	385	383
N224	1171	995	993	919	1012	1015	850	714	713	604	745	667	645	608
N584	83	18	36	71	41	93	-23	163	595	53	118	85	129	152
N1052	448	385	338	264	144	208	72	170	114	115	293	175	192	276
N1399	1888	1680	1487	1103	1086	1195	1041	878	763	775	840	676	646	641
N1404	786	576	548	414	252	419	356	345	353	269	391	274	165	190
N1407	533	564	471	399	535	454	295	54	150	320	434	162	205	193
N2681	405	256	217	169	397	458	233	110	118	102	453	304	298	324
N2768	223	111	20	63	26	45	200	-40	-28	42	123	26	112	56
N2784	209	41	70	88	58	239	95	27	94	30	88	62	82	26
N3115	554	419	572	592	419	338	454	458	457	467	446	292	330	283
N3379	826	325	350	269	107	325	136	196	156	79	231	178	132	125
N4111	233	271	52	41	20	268	249	52	-3	39	386	113	119	223
N4125	131	225	172	70	16	203	-12	30	18	104	212	144	130	141
N4278	463	436	307	330	286	318	423	248	452	231	240	244	261	387
N4374	420	216	296	221	202	427	271	217	244	302	233	135	98	54
N4382	566	216	115	-156	201	-44	93	133	85	152	317	137	27	131
N4406	205	90	210	174	104	442	242	-103	79	164	286	52	133	95
N4472	776	598	462	372	355	444	338	249	252	268	466	238	228	262
N4486	1870	892	820	801	735	950	725	598	582	543	614	479	438	464
N4494	431	143	116	81	70	107	173	243	-17	26	168	178	105	48
N4552	1061	928	811	581	644	638	611	454	459	420	524	435	381	425
N4621	404	489	340	296	260	253	265	234	408	232	246	202	242	165
N4649	1567	1361	1232	1040	978	1024	791	784	728	740	970	637	566	485
N4697	454	193	246	207	332	330	144	256	112	232	278	193	77	194
N4742	207	124	203	170	175	307	270	225	281	234	322	301	279	307
N4762	223	84	91	-1	70	195	257	101	169	-25	151	79	85	71
N4889	210	175	171	104	40	160	62	62	6	191	211	89	100	85
N5102	2313	2469	2539	2479	2626	2663	2410	2305	2339	2445	2610	2672	2488	2496
N5846	253	298	185	126	100	179	113	8	17	11	206	108	104	120
N6166	367	130	115	56	10	107	81	54	80	11	49	8	43	52

NOTE.—Flux per 50 Å interval ($\times 10^{-17}$ ergs cm^{-2} s^{-1} Å $^{-1}$).

TABLE 2B
 IUE LONG-WAVELENGTH SPECTRA, 1900 Å–3300 Å

Object	1900 2650	1950 2700	2000 2750	2050 2800	2100 2850	2150 2900	2200 2950	2250 3000	2300 3050	2350 3100	2400 3150	2450 3200	2500 3250	2550 3300	2600
N205	657	164	106	176	260	319	308	292	352	212	202	307	241	255	229
	336	416	282	281	359	428	452	404	384	571	547	362	1007	1622	
N221	118	579	319	760	971	638	872	821	812	740	627	929	732	825	957
	1838	1999	1631	1572	2458	3856	4132	3853	4576	5452	5702	5964	7736	10314	
N224	577	535	573	415	547	609	624	512	511	502	416	693	501	607	676
	1157	1227	1051	880	1147	2073	2290	2024	2322	2846	3136	3367	3992	5555	
N1052	103	423	-4	58	126	17	8	171	128	278	84	132	108	80	176
	245	225	205	238	187	313	478	363	430	625	413	482	925	1671	
N1404	130	-10	186	169	202	288	299	243	201	193	197	294	213	161	283
	309	429	302	302	360	523	817	665	668	790	989	691	816	985	
N2681	330	218	224	478	482	375	231	454	424	388	326	527	398	427	425
	692	720	621	518	797	956	1085	1083	1214	1404	1460	1150	1444	3326	
N3115	204	20	208	297	339	203	271	266	283	299	231	399	186	309	333
	568	655	530	479	614	1034	1249	1148	1247	1566	1717	1651	2150	3256	
N3379	-204	-81	129	106	167	210	260	151	184	192	128	259	167	161	237
	371	454	366	377	425	768	900	804	856	1058	1021	1092	1185	2167	
N4125	145	86	-66	-15	68	32	38	121	62	104	70	152	131	72	89
	199	268	184	148	210	350	445	354	393	544	540	445	741	572	
N4278	-239	-195	265	153	162	80	156	132	184	315	257	259	183	185	173
	267	328	249	269	268	396	493	464	509	705	688	430	1043	581	
N4374	540	59	200	116	184	246	284	112	152	194	54	255	165	117	187
	277	380	290	264	299	525	682	638	597	948	804	553	820	2998	
N4382	-6	104	251	248	311	182	183	441	254	227	483	529	240	304	346
	685	634	509	470	620	921	1130	1068	1093	1414	1498	1319	2031	5295	

TABLE 2B—Continued
IUE LONG-WAVELENGTH SPECTRA, 1900 Å–3300 Å

Object	1900 2650	1950 2700	2000 2750	2050 2800	2100 2850	2150 2900	2200 2950	2250 3000	2300 3050	2350 3100	2400 3150	2450 3200	2500 3250	2550 3300	2600
N4406	−303 241	105 252	41 251	99 218	156 265	10 505	142 490	98 417	89 511	186 701	106 593	209 453	107 1187	130 1022	158
N4472	30 377	82 474	311 401	130 388	149 414	227 680	235 866	233 723	210 802	284 1080	151 1141	361 1037	213 1653	213 1962	265
N4486	564 457	107 534	579 497	377 461	383 397	463 621	355 973	615 618	607 747	516 1034	229 882	628 −56	428 1109	368 −136	312
N4552	211 390	339 439	270 375	291 332	259 353	143 579	155 702	306 557	284 609	236 845	183 970	387 662	245 1025	294 1853	306
N4621	−614 337	540 376	327 325	513 256	409 322	−20 559	161 638	312 657	128 692	192 790	292 878	339 1156	239 1053	141 2287	258
N4649	341 414	449 442	481 384	346 363	337 431	296 615	407 739	398 603	393 628	423 846	314 894	415 651	299 1106	259 2291	352
N4762 276	−557 330	120 325	44 217	−10 319	−23 495	28 582	197 469	−46 786	25 989	14 825	177 750	144 1662	55 2320	127
N4889	647 85	394 106	−17 95	78 99	148 65	12 74	20 119	166 164	49 175	38 128	95 198	99 196	54 155	41 156	56
N5102	1854 2051	1403 2054	1836 1891	1681 1715	1907 2103	1641 2382	1426 2413	1716 2388	1740 2320	1501 2637	1363 2607	1673 2736	1664 2839	1625 2068	1654
N6166	−101 71	28 42	−63 46	−56 50	61 29	68 44	87 52	90 102	42 61	43 52	44 29	68 170	31 18	34 −89	51

NOTE.—Flux per 50 Å interval ($\times 10^{-17}$ ergs cm^{-2} s^{-1} Å $^{-1}$).

from seven lines (for the SWP exposure of NGC 4762) to 14 lines (for many images). Spectra covering 11 lines or more in extent fill the entire *IUE* aperture and have a corresponding *V* band flux through a 14" diameter circular aperture. For spectra filling less than 11 lines, a calibration of effective circular aperture size versus the number of usable lines was constructed based on the surface photometry of Lauer. It was found that 10 lines corresponds to a circular aperture of 6".9 radius; nine lines to 6".8; eight lines to 6".7, and seven lines to 6".4.

The *V* magnitude for each galaxy was calculated based on the average number of lines in the SW spectrum or spectra. For all but NGC 4762, the effective circular apertures of the LW and SW exposures are the same within 0".1 (i.e., ≤ 0.03 mag in *V*), and no adjustment was made in the relative fluxes of short and long wavelength spectra. For NGC 4762 the effective *V* magnitude of the LW spectrum is 0.12 mag brighter than that of the SW spectrum. The relative fluxes of the LW spectrum listed in Table 2B for this galaxy have been adjusted downward by 0.05 dex to correct for this difference.

V magnitudes were determined for the 14 galaxies observed by Lauer using the transformation $(V - R) = 0.91(B - V)$, as quoted in Lauer (1985). *V* magnitudes for the other 18 galaxies were determined from photoelectric circular aperture measurements and comparison to a standard elliptical galaxy growth curve (de Vaucouleurs, de Vaucouleurs, and Corwin 1976, hereafter RC2). The photoelectric data have been placed on a self-consistent magnitude system by Burstein, Marzke, and Condon (1987).

The use of an elliptical galaxy growth curve for the few S0's in this sample is justified by the small size of the *IUE* aperture: the S0's in our sample are basically bulge-dominated at this radius. Many of the magnitudes come from a recent survey of elliptical galaxies (Burstein *et al.* 1987, hereafter BDDFSLBTW). In the case of NGC 6166, the *V* flux within the *IUE* aperture was synthesized from a CCD image obtained by Lauer.

The resultant *V* magnitudes are given in Table 3. Twenty-five galaxies have photoelectric measures over a range of radii that bracket the effective *IUE* circular aperture. Of the seven galaxies requiring an extrapolation inwards of more than 0.2 mag, four are ellipticals from the BDDFSLBTW survey (NGC 2768, 4125, 4278, and 4697), for which the growth curve is known to be reliable at the *IUE* aperture based on many other elliptical galaxies. For these four and the other 25, the expected error in *V* magnitude from this interpolation or extrapolation is typically less than ± 0.05 mag. The remaining three galaxies are either S0's (NGC 2784 and NGC 4111) or an Sa (NGC 2681), for which the growth curves are less well known and the inward extrapolation of *V* magnitude to the effective aperture is also greater than 0.8 mag. The expected errors in *V* for these three objects are estimated to be 0.15 mag and are noted in Table 3.

The above estimated error in *V* must be combined with possible systematic errors of $\pm 0".5$ in the *IUE*-circular effective aperture conversion and with centering uncertainties of *IUE* of a similar size. With all probable sources of error included, the error in *V* magnitude relative to *IUE* is expected to be < 0.1 mag for 29 galaxies and < 0.2 mag for the other three.

d) Structure and Stellar Population Parameters

Most values of Mg_2 and central velocity dispersion have been taken from the elliptical galaxy survey published by Davies *et al.* (1987). For S0 galaxies and M31 these parameters have been determined from Lick ITS spectra in a similar manner. The use of Mg_2 to rank order the line strengths and metallicities of old stellar populations is well established (e.g., Burstein *et al.* 1984). Likewise the velocity dispersion, σ , is both a measure of the depth of the central gravitational field and of the total luminosity of elliptical galaxies (Faber and Jackson 1976).

The Mg_2 index is defined by Faber *et al.* (1985). As used here, Mg_2 has been combined with Mg_1 to produce a modified Mg_2

TABLE 3
GLOBAL PARAMETERS FOR PROGRAM GALAXIES

Name (NGC) (1)	<i>T</i> (2)	<i>A_B</i> (3)	<i>V</i> (4)	$\log f_{\lambda}(V)$ (5)	M_{G_2} (6)	Velocity (7)	$\log \sigma$ (8)	1550 (9)	(1550 - <i>V</i>) (10)
205	S	0.14	13.49	-13.760	0.071	-239	...	-14.237	1.19
221	Q	0.31	10.30	-12.433	0.198	-199	1.90	-14.234	4.50
224	Q	0.31	10.28	-12.425	0.324	-300	2.18	-13.829	3.51
584	Q	0.12	12.25	-13.270	0.298	1875	2.36	-14.844	3.93
1052	A	0.06	12.45	-13.369	0.318	1475	2.33	-14.593	3.06
1399	Q	0.00	11.88	-13.159	0.357	1447	2.52	-13.979	2.05
1404	Q	0.00	11.73	-13.099	0.344	1941	2.39	-14.419	3.30
1407	Q	0.16	12.55	-13.378	0.341	1764	2.48	-14.337	2.40
2681	S	0.09	12.09	-13.215	0.153	710	2.02	-14.489	3.18
2768	Q	0.16	12.76	-13.462	0.296	1363	2.32	-15.023	3.90
2784	Q	0.66	12.15	-13.067	0.334	708	2.41	-14.527	3.65
3115	Q	0.10	11.33	-12.908	0.309	698	2.45	-14.282	3.43
3379	Q	0.05	11.58	-13.024	0.329	895	2.33	-14.569	3.86
4111	Q	0.00	11.80	-13.127	0.274	794	2.15	-14.832	4.26
4125	Q	0.04	12.59	-13.431	0.312	1340	2.38	-14.914	3.71
4278	A	0.10	12.18	-13.248	0.293	627	2.45	-14.400	2.88
4374	Q	0.13	11.83	-13.099	0.323	1034	2.48	-14.518	3.55
4382	Q	0.04	11.84	-13.131	0.242	773	2.24	-14.818	4.22
4406	Q	0.11	12.15	-13.233	0.330	-243	2.42	-14.720	3.72
4472	Q	0.00	11.62	-13.055	0.331	1018	2.49	-14.421	3.42
4486	A	0.08	12.15	-13.243	0.303	1305	2.60	-14.059	2.04
4494	Q	0.06	12.32	-13.317	0.293	1350	2.12	-14.825	3.77
4552	Q	0.14	12.01	-13.168	0.346	340	2.44	-14.109	2.35
4621	Q	0.07	12.06	-13.210	0.355	444	2.41	-14.483	3.19
4649	Q	0.03	11.79	-13.114	0.360	1114	2.56	-14.011	2.24
4697	Q	0.04	12.11	-13.239	0.320	1231	2.25	-14.602	3.41
4742	S	0.09	12.35	-13.319	0.192	1289	2.00	-14.542	3.06
4762	Q	0.04	12.61	-13.439	0.280	945	2.11	-14.924	3.71
4889	Q	0.05	13.49	-13.788	0.356	6441	2.60	-14.884	2.74
5102	S	0.20	11.94	-13.122	0.084	420	1.85	-13.445	0.80
5846	Q	0.14	12.90	-13.524	0.340	1709	2.46	-14.769	3.11
6166	A	0.00	14.65	-14.267	0.324	9385	2.53	-15.081	2.04

NOTES TO TABLE 3

- COL. (2).—Classification based on optical spectra and imaging: Q = quiescent; A = active; S = star-forming.
 COL. (3).—Galactic extinction, taken from Burstein and Heiles 1984.
 COL. (4).—*V* magnitude within *IUE* aperture.
 COL. (5).—Logarithm of flux, in $\text{ergs cm}^{-2} \text{s}^{-1} \text{\AA}^{-1}$, corresponding to *V* magnitude.
 COL. (6).—Absorption-line strength, in mag.
 COL. (7).—Heliocentric radial velocity.
 COL. (8).—Logarithm of central velocity dispersion.
 COL. (9).—Logarithm of flux, in $\text{ergs cm}^{-2} \text{s}^{-1} \text{\AA}^{-1}$, from 1250 to 1850 \AA .
 COL. (10).—Ratio of the 1550 flux to the *V* flux, expressed in terms of magnitudes.

index that is more accurate but still on the same scale as the original (see discussion by Davies *et al.* 1987). The measurement of velocity dispersions from the Lick ITS spectra is described by Dalle Ore *et al.* (1988) and summarized in the discussion of Davies *et al.* The typical error of M_{G_2} for this study is ± 0.007 mag, and the error in $\log \sigma$ is ± 0.03 dex. Absolute luminosities are not calculated directly for these galaxies, owing to the known uncertainty in Hubble distances for nearby galaxies (cf. Lynden-Bell *et al.* 1988). Rather, the well-established correlation of σ with total luminosity for ellipticals is used to substitute for total luminosity in the correlations discussed below.

e) Reddening, Extinction, and Redshift Corrections

The reddenings for all galaxies come from Burstein and Heiles (1984). As described there and in Burstein and Heiles (1982), the accuracy in $E(B-V)$ north of declination -23° is 0.01 mag or 10% of the reddening, whichever is larger. The accuracy south of -23° is 0.03 mag owing to lack of information on the local gas-to-dust ratio there. Fortunately, all of the

galaxies in the present sample south of -23° are in areas of little or no reddening. Values of $E(B-V)$ are given in Table 3.

The analytic model of Seaton (1979) was used to calculate the extinction at *V* and at the *IUE* wavelengths. This model uses $A_V/E(B-V) = 3.10$ and is close to the preferred curve of Savage and Mathis (1981) except near the 2200 \AA "bump," where it deviates by 5%. As the most reddened galaxy in our sample has $E(B-V) = 0.17$ mag, this difference is less than 0.03 mag at 2200 \AA , too small to matter. The (1550 - *V*) colors in Table 3 have been corrected for extinction.

The ultraviolet spectra in Tables 2A and 2B have been flux-averaged in each 50 \AA interval, extinction-corrected and deredshifted. The heliocentric radial velocities for each galaxy are given in Table 3. Flux ratios are expressed as $\log(f_u/f_v)$ in 50 \AA intervals and are used in the following figures.

f) Error Summary for UV Data

A realistic estimate of the errors in the ultraviolet and visual fluxes is important for the following discussion. The error in the (1550 - *V*) color is a product of errors in *V* magnitude

(0.10–0.2 mag), galactic extinction (<0.06 mag), random errors in the 1550 flux (ranging from <0.01 dex for the highest observed flux to 0.04 dex for the lowest observed flux), and systematic errors in the instrumental level of SW flux owing to imperfect background subtraction. To estimate the size of this latter effect, a series of test reductions was performed on blank regions alongside the real spectrum. These tests indicated systematic errors that could vary the 1550 flux of the brightest UV source by up to 0.01 dex and that of the faintest sources by up to 0.10 dex. These errors are consistent with previous average estimates of ~ 0.02 dex (Holm *et al.* 1982) errors for bright sources due to systematic effects, as well as effects due to the “fixed-pattern” noise that is known to exist in the SWP camera (Hackney, Hackney, and Kondo 1982). Taking all of these together, we conservatively estimate a combined error of 0.17 mag in $(1550 - V)$ color for 28 of the galaxies, and 0.25 mag for NGC 2681, NGC 4111, NGC 2784 and NGC 6166.

The errors in $\log(f_{\lambda}/f_V)$ include all the above terms plus the uncertainty due to the match between the SW and LW spectra. The fixed-pattern noise in the SWP is a series of sharp spikes in the spectra that, at 50 Å resolution, result in excess flux near 1300, 1500, 1570, 1660, 1750, and 1880 Å, with the most prominent effect near 1750 Å (Hackney, Hackney, and Kondo 1982). The amplitude of this pattern appears to vary considerably, typically 0.03 dex for the brighter galaxies and >0.3 dex for the faintest galaxies. The match between the SW and LW spectra should be accurate to ≤ 0.02 dex. Finally, the absolute flux errors are comparable to those for $(1550 - V)$ given above. These estimates for random and systematic errors in $\log(f_{\lambda}/f_V)$ are consistent with visual intercomparisons of short and long exposures for the same objects.

III. GENERAL TRENDS

a) *The Relationships among $(1550 - V)$, σ , L , and Mg_2*

Diagrams correlating Mg_2 and central velocity dispersion with $(1550 - V)$ are given in Figures 1a and 1b. In both figures, the sample has been divided into three classes: (1) 24 elliptical and S0 galaxies (including the nucleus of M31) whose optical spectra show little or no evidence for either star formation or nuclear emission. These “quiescent” or normal galaxies (*closed squares*) form the backbone of the sample. (2) Four “active” elliptical galaxies with strong nuclear emission—NGC 1052, 4278, 4486, and 6166 (*open squares*). (3) Four “star-forming” galaxies with recent nuclear star formation, as inferred from optical spectra (*crosses*; NGC 205, 2681, 4742, and 5102; see the Appendix).

The 24 quiescent galaxies exhibit a well-defined, curved relationship between Mg_2 and $(1550 - V)$ color and scatter that is consistent with observational error. The general form of this relationship is similar to that suggested by Faber (1983) and establishes that the level of far-ultraviolet emission from old, quiescent stellar populations is not a random variable but becomes *bluer* with increasing absorption-line strength (metallicity). This finding is the major observational result of this paper and confirms the presence of a *systematically varying* hot component in old stellar populations that dominates the far-ultraviolet flux.

It is significant that the two classes of galaxies with known spectral peculiarities are well separated from the main Mg_2 – $(1550 - V)$ relationship and also from each other: The four star-forming galaxies have blue $(1550 - V)$ magnitudes

and very low values of Mg_2 that strongly distinguish them from the main relation. The residuals of the active galaxies are smaller but are systematic in sign and are individually larger than the observational errors. That four objects that are distinguished *a priori* by strong nuclear emission could display such behavior purely by chance seems to us rather improbable. As discussed below, two of these objects may also share a spectral anomaly. For these reasons, we have tentatively concluded that the four active galaxies also represent a separate class and discuss them apart from the other objects.

The companion diagram correlating central velocity dispersion with $(1550 - V)$ color (Fig. 1b) shows the same general relationship as Figure 1a for the quiescent galaxies and the star-forming galaxies but with less of a distinction between active and quiescent galaxies. The well-known correlation of absolute luminosity with central velocity dispersion (e.g., Faber and Jackson 1976) implies that absolute luminosity should also correlate with $(1550 - V)$ color (in the sense of higher luminosity galaxies being bluer). Although the distances and absolute luminosities of ellipticals can be calculated in a variety of ways, the scatter in L – $(1550 - V)$ relationship is also large, regardless of how L is derived: from raw Hubble velocity, Hubble velocity corrected for a model inflow pattern (Lynden-Bell *et al.* 1988) or distances as estimated by Lynden-Bell *et al.* (1988). All these methods have been tried but are not shown here for brevity.

That the scatter for quiescent galaxies is low in Figure 1a suggests that the $(1550 - V)$ – Mg_2 correlation is the most direct physical correlation. The larger scatter in the color– $\log \sigma$ and color– L diagrams can be understood to result from the σ – Mg_2 and L – Mg_2 relations, which show a trend, but with intrinsic scatter (e.g., Burstein *et al.* 1988). Since Mg_2 is thought to measure metallicity in old stellar populations (e.g., Burstein *et al.* 1984), the further implication is that metallicity is the fundamental underlying physical variable in the $(1550 - V)$ – Mg_2 relation.

In other words, the UV flux in quiescent galaxies depends on a property of the stellar population itself rather than on some dynamical structural parameter of the galaxy. This is the principal conclusion of this section.

b) *Ultraviolet Spectral Energy Distributions*

Ultraviolet spectra are presented for 27 galaxies in Figures 2a–2h. The spectra have been arranged in groups according to their positions in the Mg_2 – $(1550 - V)$ diagram. The first five panels (Figs. 2a–2e) show quiescent galaxies, arranged by $(1550 - V)$ from bluest to reddest (the active galaxies NGC 1052 and NGC 4278 are also included in Fig. 2b; see below). It is seen that quiescent galaxies with similar $(1550 - V)$ have similar spectral energy distributions (SEDs) from 1200 to 3200 Å. Furthermore, as the level of far-UV emission increases between 1200 and 1900 Å, the slope of the increasing flux below 1600 Å remains approximately the same. A mean SED for the four bluest galaxies in Figure 2a is repeated in the other figures to guide the eye.

Even at this low resolution, prominent absorption-line features are visible in essentially all of the quiescent galaxy spectra from 2600 to 3200 Å. These lines correspond to strong absorption features in F–G stars, as displayed in the *IUE Spectra Atlas* (Wu *et al.* 1983). In contrast to these obvious features, identification of any absorption lines below 2000 Å is much more uncertain. Figure 3 shows the weighted average SW spectra of M31 and the combined SW spectrum of NGCs 1399,

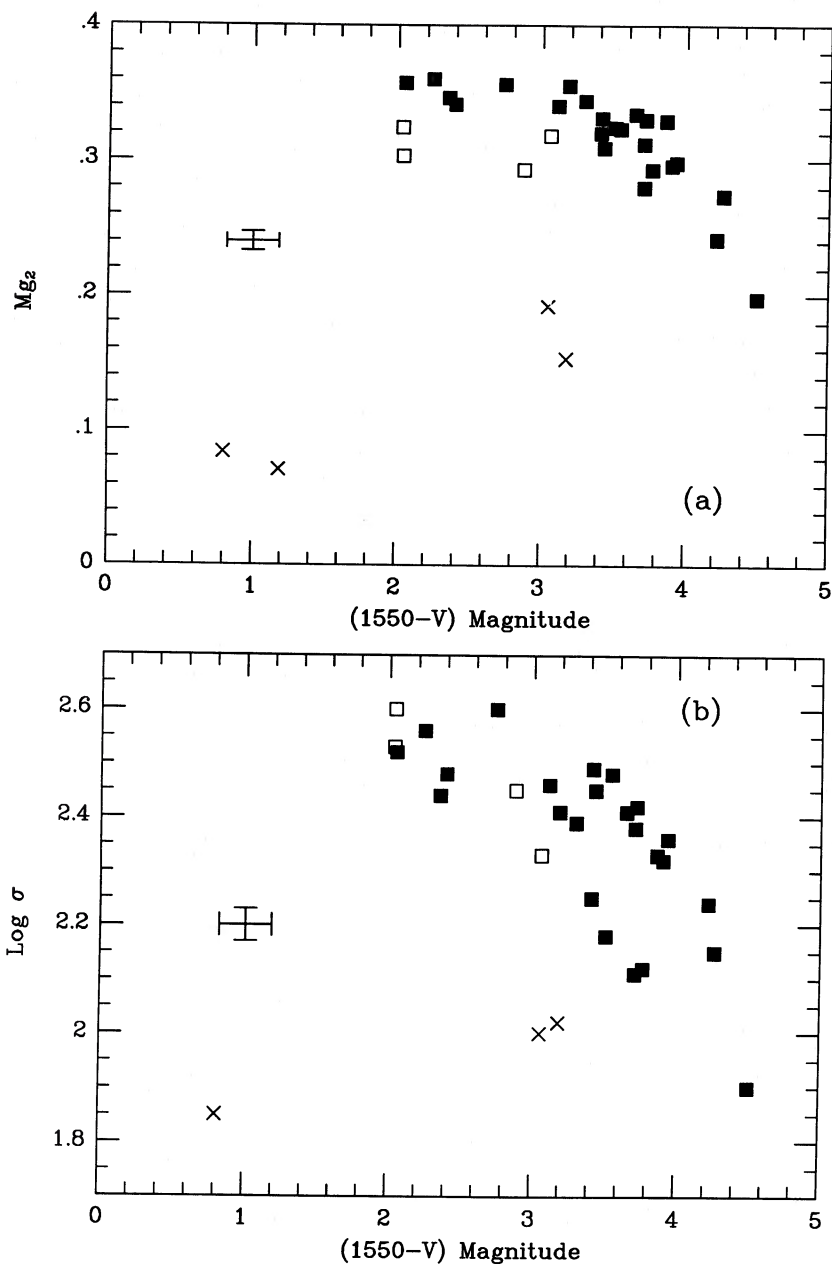


FIG. 1.—(a) The optical absorption-line index Mg_2 plotted vs. the ultraviolet/optical $(1550 - V)$ color (expressed in magnitudes) for the 32 galaxies in this sample. Closed squares represent “quiescent” galaxies, open squares represent “active” galaxies, and crosses represent galaxies with on-going star formation. (b) Central velocity dispersions for 31 of the galaxies (NGC 205 excepted) vs. $(1550 - V)$ color. Along with larger intrinsic scatter, there is no separation of active and quiescent galaxies in this plot.

4552, and 4649. An average of main-sequence B1–1.5 V stars (Fanelli, O’Connell, and Thuan 1987) is also plotted for comparison, with the positions of the strongest spectral-line features marked.

As previously noted by Welch (1982), the SW spectrum of M31 shows strong Si II 1260 Å and 1304 Å and C II 1335 Å absorption lines. On the other hand the summed spectrum of the giant ellipticals shows very weak lines, if any at all. While the lack of a strong C IV 1550 Å absorption feature excludes the presence of stars B0 and earlier (Fanelli, O’Connell, and Thuan; Welch 1982), all four strong UV lines are strong interstellar features (Savage and de Boer 1981; Welch 1982). Equivalent widths even in high-latitude stars often exceed 1 Å

(Savage and de Boer 1981). The equivalent widths in Figure 3 in M31 are of order 2–3 Å, which are perhaps not inconsistent with its low galactic latitude and high extinction. The SW spectra of giant ellipticals may be similarly contaminated (e.g., weak absorption near Si II 1304). To summarize, the high-resolution spectra are inconclusive but do not strongly support the presence of very hot young stars in quiescent galaxies.

Figures 2f and 2g show the star-forming galaxies grouped into pairs by mean UV color. The SEDs for the two bluer ones (NGC 205 and NGC 5102) are remarkably flat, varying little in relative flux from 1200 to 3000 Å and by only a factor of 2–3 relative to the V passband. Note that the IUE spectrum of NGC 205 did include regions containing O stars.

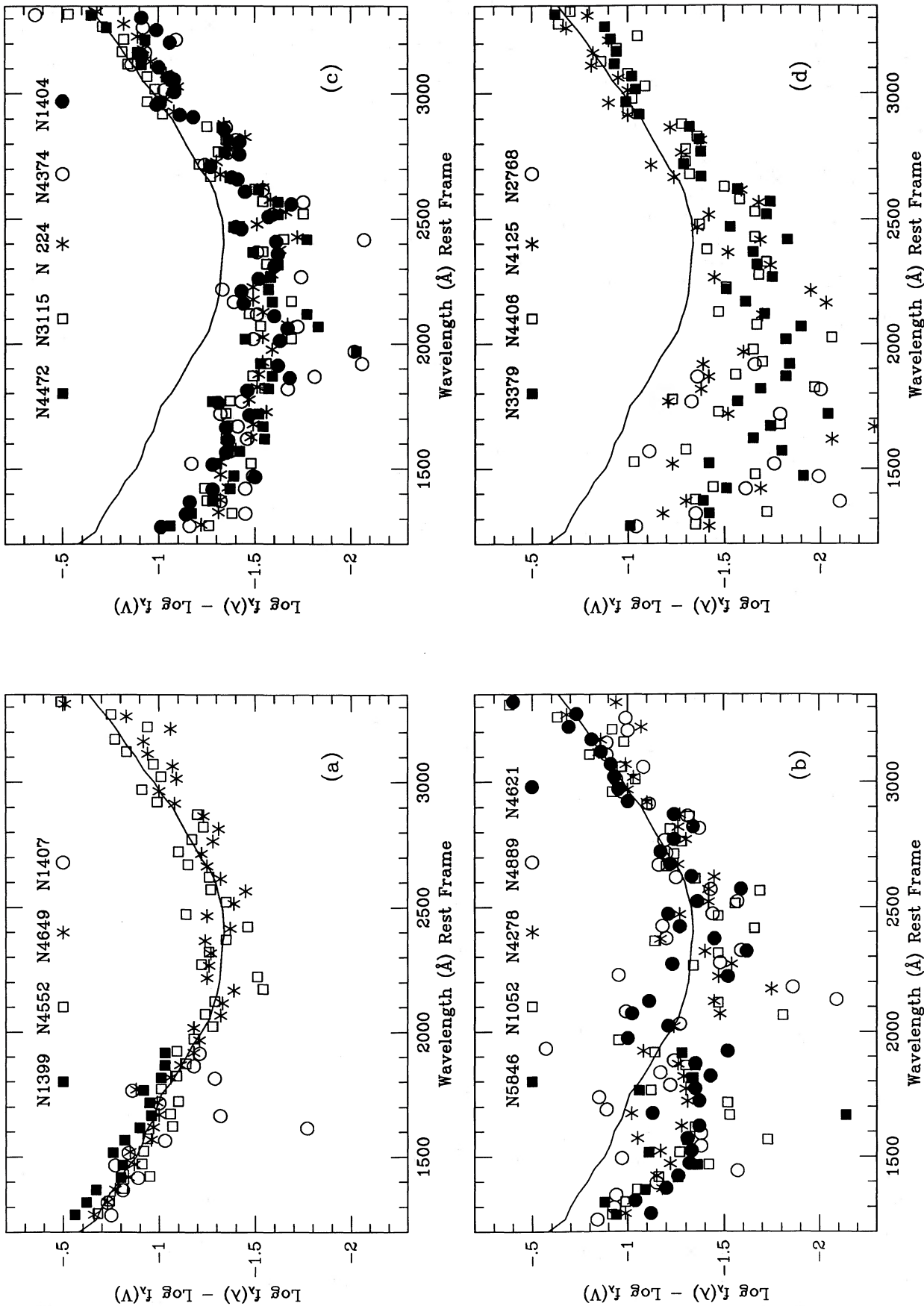


FIG. 2.—Eight panels plotting the reddening-corrected and redshift-corrected ultraviolet spectra for 27 of 32 galaxies in this sample. All spectra are plotted as $\log f_{\lambda} - \log f_{\nu}$ vs. wavelength and are divided according to their position in the $(1550 - V)$, Mg_2 diagram (Fig. 1*a*). (a) The four quiescent galaxies with the bluest $(1550 - V)$ colors. (b), (c), (d), and (e): 15 quiescent and two active galaxies, arranged in order of $(1550 - V)$. Note the high degree of similarity of the ultraviolet spectra of quiescent galaxies with similar values of $(1550 - V)$ and Mg_2 . (f) The two bluest star-forming galaxies. (g) The two reddest star-forming galaxies. (h) The two active galaxies with the bluest $(1550 - V)$ colors; note possible excess emission from 2000 to 2500 \AA with respect to blue quiescent galaxies.

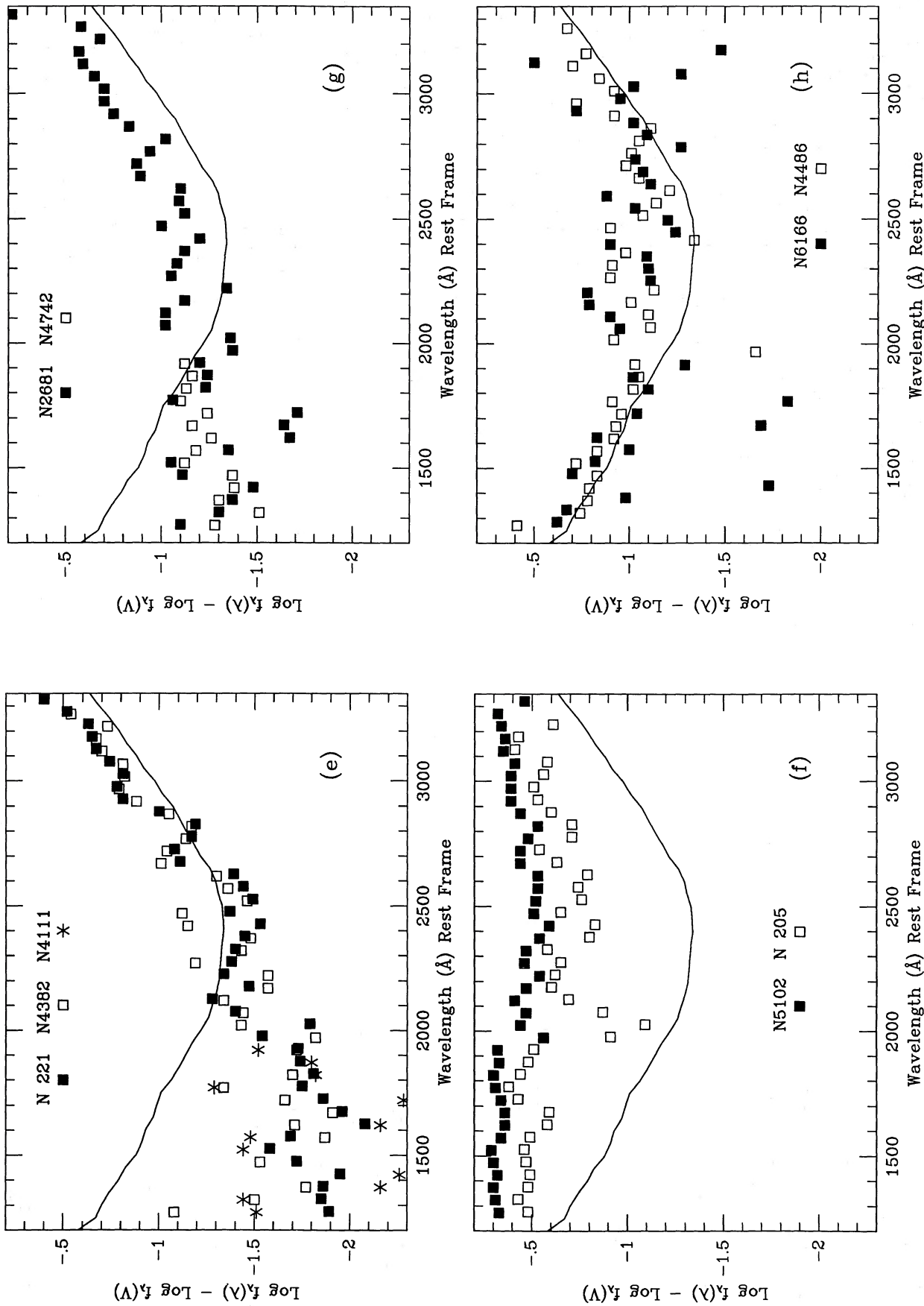


FIG. 2—Continued

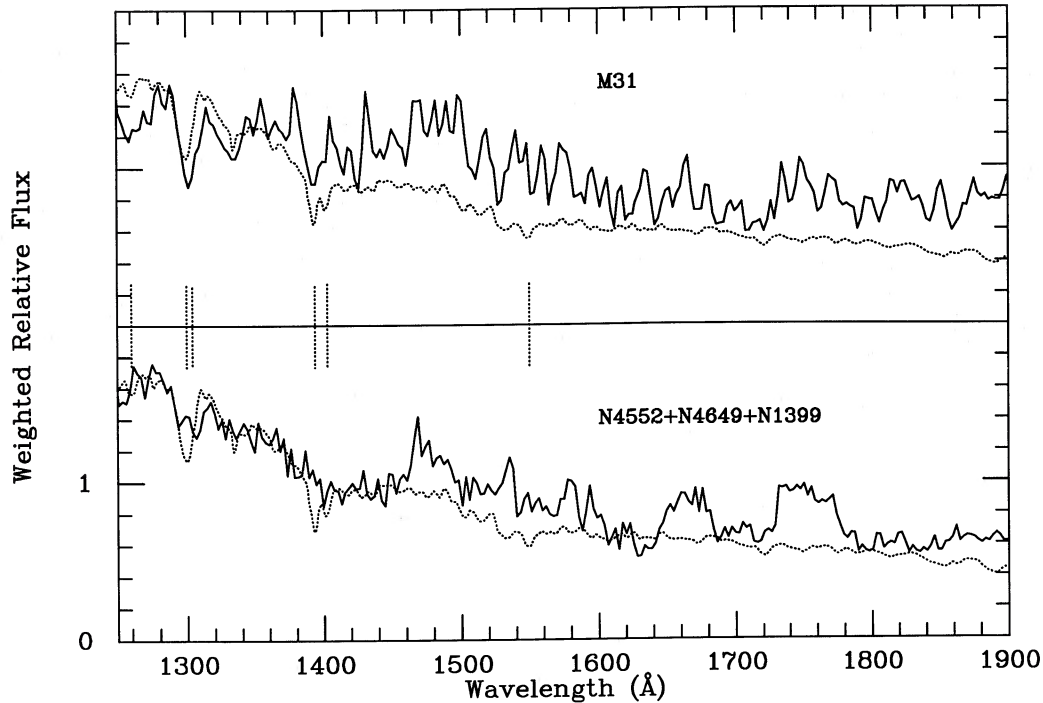


FIG. 3.—SWP low-resolution spectra plotted at high resolution for the center of M31 (=NGC 224) (*upper panel*) and the weighted sum of NGC 1399, 4552, and 4649 (*lower panel*). The mean spectrum of B1–1.5 V stars, from Fanelli, O’Connell, and Thuan (1987) is plotted over both spectra (*dotted line*). Positions of prominent absorption lines in early-type stars are marked: The Si II and S II blend at 1260 Å; the 1300 and 1304 Å lines of Si II and Si III; the 1394 and 1403 Å lines of Si IV and the 1550 Å line of C IV. The strong features near 1300 Å and 1400 Å in the spectrum of M31 may be contaminated by interstellar lines.

The SEDs for the two redder star-forming galaxies (NGC 2681 and NGC 4742) actually *decline* at the shortest wavelengths, in strong contrast to the far-UV blue slope in all the other galaxies. This indicates a relative deficiency of hot OB stars compared to later type stars. The SED of NGC 2681 is notably different from NGC 5102 and NGC 205 in showing a strong overall decrease in flux from the *V* passband to 1200 Å.

As in quiescent galaxies, absorption-line complexes from 2600 to 3200 Å are visible in the star-forming galaxies, although their strength is somewhat diluted by the young stellar population. In addition, Si II, Si III, and C IV absorption lines are visible in the original spectrum of N5102, similar to those shown by B main-sequence stars of Figure 3 (see, however, the discussion above about possible interstellar contamination).

Figure 2*h* shows spectra of the two bluest active galaxies (NGC 4486 and NGC 6166). Although their (1550 – *V*) colors are similar to those of blue quiescent galaxies, these active galaxies may have excess flux in the dip near 2300 Å (compare with the mean line from Fig. 2*a*). This could imply an additional, or perhaps a completely different, hot component, one with excess flux at 2300 Å relative to shorter wavelengths (e.g. a power law, or perhaps the “blue bump” that is seen in the spectra of Seyfert galaxies Malkan and Sargent 1982). If the entire light of the semistellar nucleus in NGC 4486 were synchrotron radiation, with spectrum $f_\nu \approx \nu^{-0.7}$ and $V = 16.5$ (Young *et al.* 1978), this spectrum would match perfectly the excess flux at 2300 Å. However, from absorption-line strengths in the nuclear spike, Dressler (1980) limits the *V* mag of any nonthermal component to less than one-fifth this level, in which case the excess cannot be synchrotron radiation for any plausible spectral index.

The two redder active galaxies (NGC 1052 and 4278) are

compared to the intermediate quiescent galaxies NGCs 4889 and 4621 in Figure 2*b*. No similar deviation at 2300 Å is obvious there; whether by reason of poor *S/N* or real absence is not clear.

To summarize the major conclusions of this section:

1. The UV spectra of quiescent early-type galaxies appear to form a continuum in which the major variable—amplitude of the hot, blue component—is positively correlated with Mg_2 strength.
2. The UV spectra of star-forming early-type galaxies are qualitatively different, being flatter or monotonically declining toward the shortest wavelengths.
3. High-resolution UV spectra of the bluest quiescent galaxies lack absorption lines of hot main-sequence stars, whereas such lines may be present in M31. However, these lines are also produced in interstellar gas, and it is possible that the observed features in M31 are affected by interstellar components in our own Galaxy.
4. There is tentative evidence that the SEDs of at least two active galaxies, NGC 6166 and NGC 4486, differ systematically from those of quiescent ellipticals. These two galaxies appear to show excess flux near 2300 Å.

IV. THE ULTRAVIOLET SPECTRA OF “QUIESCENT” EARLY-TYPE GALAXIES

The remainder of this paper is concerned with population models for the UV flux. Numerous investigators have already presented a wide variety of such models (e.g., Wu *et al.* 1981; Perola and Tarenghi 1980; Oke, Bertola, and Capaccioli 1981; Fosbury *et al.* 1981; Nesci and Perola 1985; Bertola *et al.* 1986; Kjaergaard 1987; Rocca-Volmerange and Guiderdoni 1987), but the approach we take here is slightly different. Guided by the newly discovered systematic UV properties of quiescent

galaxies, we use these objects as a basic ingredient in models for star-forming and active galaxies. We likewise make use of UV-poor quiescents as a starting point to model UV-bright ones. This approach is similar to Gregg's (1985) analysis of S0 disks, which utilized the spheroidal populations of E's and S0's as a springboard. The spectra of the star-forming galaxies are considered separately in the Appendix.

a) *The Composite Nature of the UV Spectra*

The UV flux distributions from 1200 to 3200 Å appear to be the sum of two components of distinctly different energy dis-

tributions (cf. Oke, Bertola, and Cappaccioli 1981; Welch 1982). The first is very red in color, primarily due to main-sequence stars. Standard stellar population models of ellipticals predict that the wavelengths from 2600 to 3200 Å are dominated by the light of turnoff F-G dwarfs, with a small contribution from K giants. The F-G dwarf stars exhibit prominent absorption complexes at 2650 Å, 2850 Å, and 3050 Å due to Mg II and iron-peak elements characteristic of F-G dwarfs (Wu *et al.* 1983). These absorption lines appear in the spectra of all the quiescent galaxies.

The second spectral component is quite blue with a steep

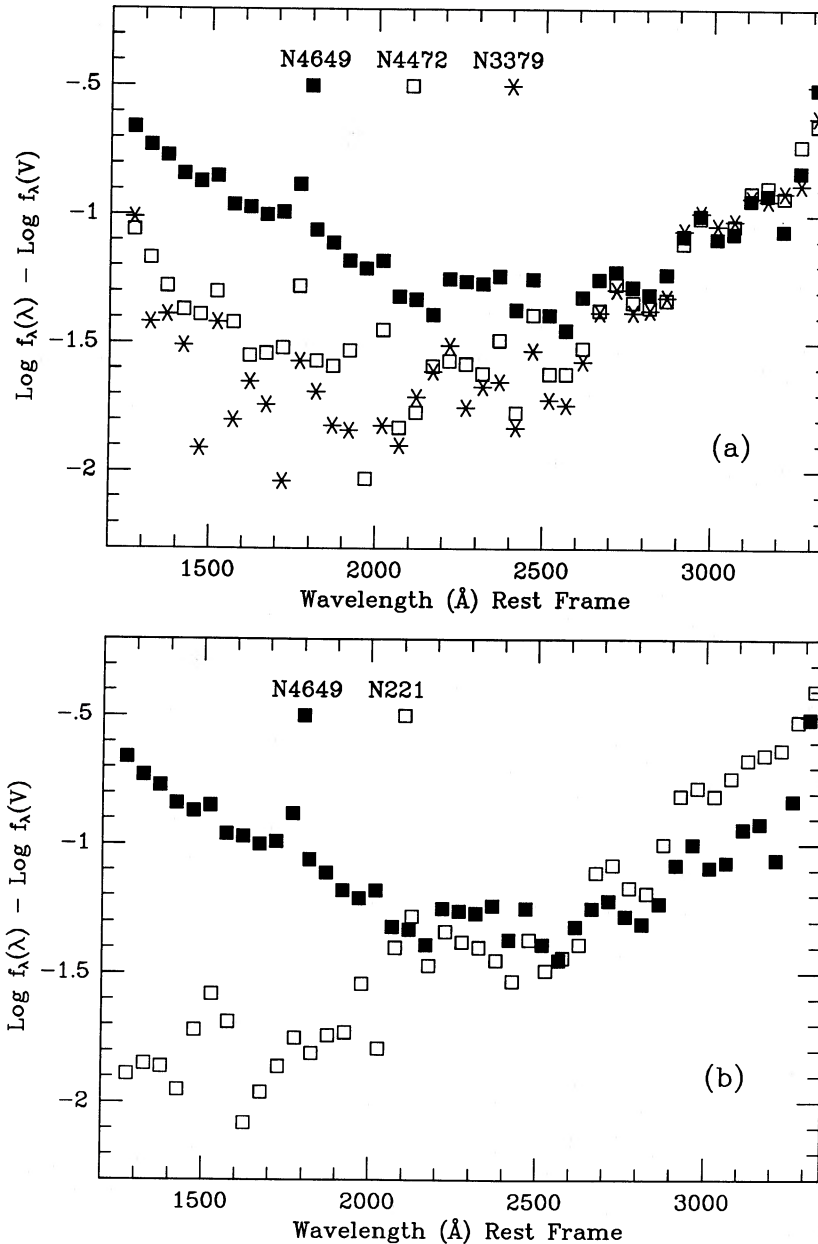


FIG. 4.—(a) Ultraviolet energy distributions of three quiescent galaxies that span the maximum range in Mg_2 . All three galaxies have similar energy distributions from 2600 to 3200 Å, despite a relatively wide intrinsic range in the strengths of optical absorption-line features. This demonstrates that the blue light contamination in these galaxies is significant even at 3000 Å (see also Fig. 8). (b) The quiescent galaxy with the strongest optical absorption lines, N4649, vs. the galaxy with the weakest lines, NGC 221. The cross-over of the ultraviolet spectra further demonstrates the measurable amount of blue light contamination near 2600 Å in NGC 4649.

slope toward the far-UV. One infers from Figure 2 that the large variation in $(1550 - V)$ among quiescent galaxies is due to a large change in the amplitude of this blue component relative to the red one.

To illustrate these points, Figures 4a and 4b compare an SED of a galaxy that is representative of the class of ellipticals with the strongest measures of Mg_2 to those of ellipticals with lower metallicities. Note the similarity of the SEDs longward of 2700 Å versus their divergence shortward of that wavelength. The enormous color change in the UV is by far the largest yet observed in any wavelength region among early-type galaxies, whose spectra in other wavelength regions are otherwise homogeneous to within a few tenths of a magnitude.

A major point, which we demonstrate explicitly in § IVc, is the fact that UV quiescent spectra are highly composite over the entire wavelength range from 2000 to 3200 Å. Both hot and cool components contribute, and variations in the hot UV flux can mask the effect of metallicity differences in the turnoff stellar populations. In fact, the apparently small range of the $(2800 - V)$ colors of quiescent galaxies is largely an artifact of the playing off of the hot component against the metal dependence of the cool component. The highly composite nature of the UV spectrum below 3200 Å has not been generally appreciated before (e.g., Rocca-Volmerange and Guiderdoni 1987).

Both theory and Figure 8 below indicate a strong dependence of the red component on composition (and hence Mg_2) through line-blanketing and main-sequence turnoff color. Both of these effects redden the turnoff stars and depress the flux from 2000 to 3200 Å. A reliable model for the underlying red component contributing to the ultraviolet is therefore a necessity. Unfortunately, model atmospheres over a wide range in metallicity are virtually untested in the UV, and the empirical library of stars currently available from *IUE* is also inadequate. Even if all the machinery were in place, we would still lack a reliable calibration to translate differences in Mg_2 into differences in $[Fe/H]$, a transformation that is, in our opinion, still highly uncertain.

The most pragmatic approach at the moment is to model these spectra differentially, i.e., to use certain UV-red galaxies as basic templates for bluer objects. Given the probable intrinsic range of metallicity among the red population, this approach cannot be pushed too far, but it is still instructive. Two models that are representative of two current modes of thought on the origin of the hot stellar population are detailed here: (1) a continuing star formation model that can be explicitly compared to the predictions of star formation resulting from X-ray cooling flows; and (2) post-asymptotic giant branch (PAGB) models that can be compared to current theoretical predictions of the systematics of PAGB evolution.

b) Two Stellar Population Models

i) Continuing Star Formation

Continuing star formation models have been calculated by Bruzual (1983) and by B. M. Tinsley (1980, private communication) under a variety of assumptions for the time scale of ongoing star formation and canonical initial mass functions. For the present analysis we use a model from Tinsley which has continuing star formation over a 10 Gyr period, and a model from Bruzual for a 16 Gyr period. As the UV spectra of continuing star formation models change little past an age of 5 Gyr (Bruzual 1983), the precise length of time of continuing star formation is important only in determining the level of UV flux, not its spectral distribution.

Figure 5 shows the UV SEDs for these two models as $\log f_\lambda/f_V$. The two are fairly similar. The Tinsley model has been constructed from *ANS* broad-band fluxes (which we have corrected for *IUE-ANS* zero-point differences using stars in common), while the Bruzual models are based on the higher resolution *IUE* data. The differences between the two models may be taken as an indication of the uncertainty of the modeling process.

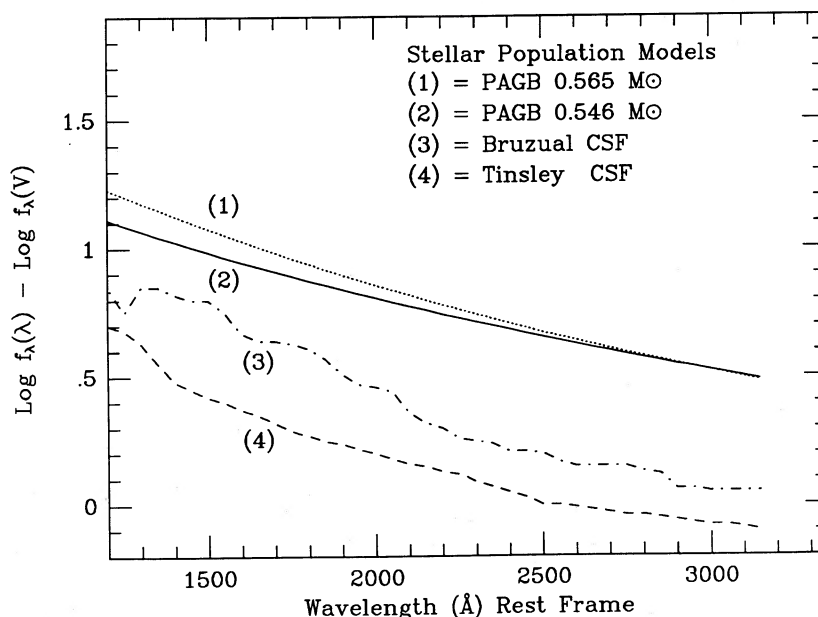


FIG. 5.—The ultraviolet energy distributions of the four hot stellar population models used in this paper and described in the text. Note the similar ultraviolet shapes for all four models but the different $(1200 - V)$ colors.

ii) PAGB Models: Planetary Nebula Nuclei

No composite model of the integrated ultraviolet flux from the PAGB phases has yet been calculated, although the ultraviolet flux from representative stars has been used in previous models (e.g., Wu *et al.* 1980; Gunn, Stryker, and Tinsley 1981). Here we use models calculated by Schoenberner (1983), giving values of $\log T_e$ and $\log L_{\text{bol}}$ versus evolutionary time for core masses of 0.546 and $0.565 M_{\odot}$. The evolutionary tracks for each mass were divided into 23 discrete intervals, each specified by an average $\log T_e$, $\log L_{\text{bol}}$, and the time spent at those values. Blackbody spectra were calculated for each value of

$\log T_e$ and co-added, weighted by the product $L_{\text{bol}} \times t$ of that phase.

The resulting composite spectra are shown in Figure 5. The two different masses produce very similar spectral energy distributions, but the efficiency of UV light production is substantially different. The lower mass star produces nearly 6 times the total V luminosity despite its having much lower L_{bol} . This is due to a much greater hydrogen envelope mass and hence greater total time spent in the planetary phase, as noted by Renzini and Buzzoni (1986). The extreme sensitivity of integrated luminosity to core mass is one of the most striking features of PAGB models and discussed further in § VI.

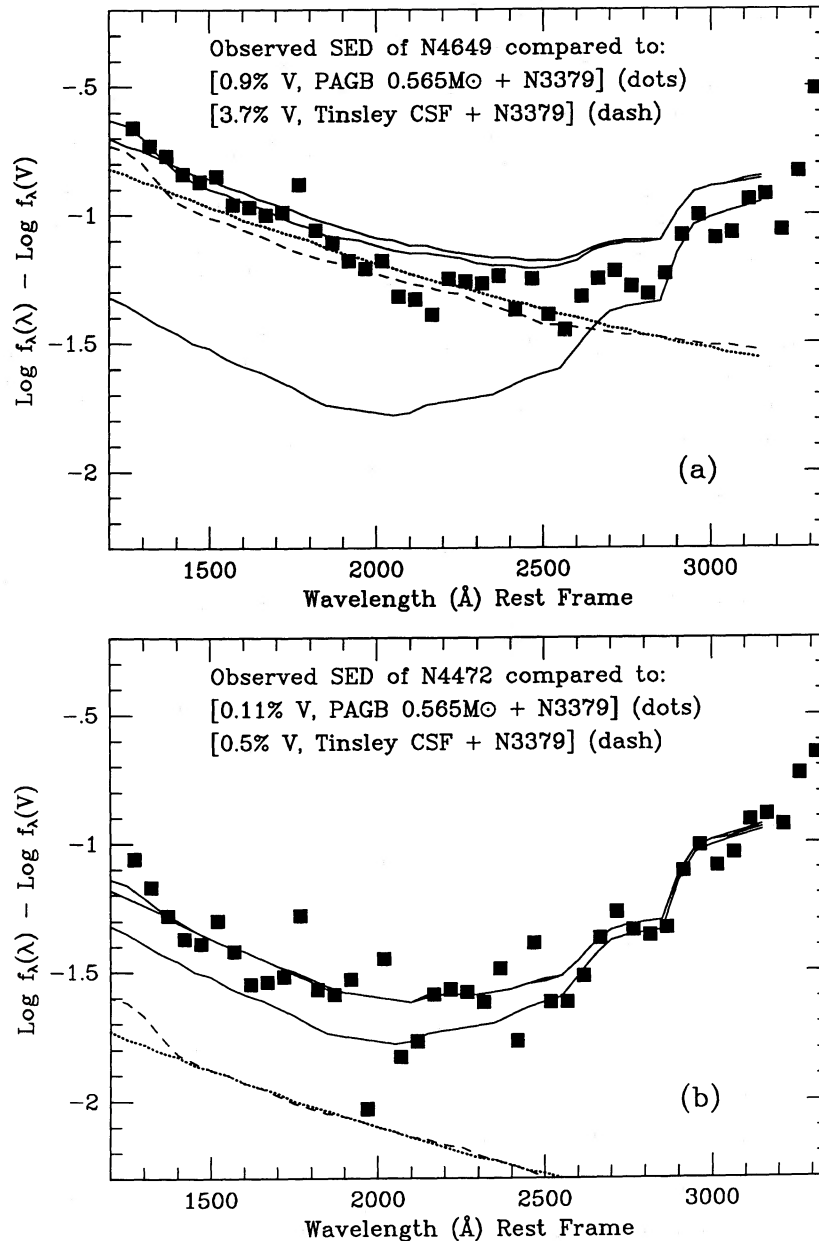


FIG. 6.—Composite models based on the observed energy distribution of NGC 3379 plus two kinds of hot stellar populations are compared to ellipticals with blue UV energy distributions. (a) The PAGB $0.565 M_{\odot}$ and the CSF Tinsley model added to NGC 3379 are compared to NGC 4649. The bottom solid line is the SED of NGC 3379, the dotted line is the PAGB model flux, the dashed line is the CSF model flux, and the two upper solid lines are the resulting model SEDs. (b) As in (a), but compared to NGC 4472, with proportionally lower levels of UV contamination.

c) Model Fits to the UV SEDs of Quiescent Galaxies

The slope of the SEDs for the above two models are similar to each other and to the far-UV observed SEDs of elliptical galaxies. However, the relative contributions to V light in the PAGB models are about a factor of 5 less than for the continuing star formation (CSF) models (see Fig. 5). Thus, for the same total amount of UV flux, the PAGB model is better "hidden" in the optical spectrum.

Figures 6a and 6b present model fits to the spectra of two metal-rich ellipticals. A smoothed representation of the energy distribution of NGC 3379 (*lower solid line* in both figures) is used as the base template for the (mostly) cool population, to which is added flux from either a Tinsley CSF model (*dashed line*) or a $0.565 M_{\odot}$ PAGB model (*dotted line*). The sum of model + NGC 3379 (*two upper solid lines* in both figures) is then plotted over the observed SEDs of NGC 4649 (Fig. 6a) and NGC 4472 (Fig. 6b).

The model + NGC 3379 is a very good fit to the SED of NGC 4472 over the whole UV spectrum for either model energy distribution. In contrast, the model + NGC 3379 for NGC 4649 fits well only at wavelengths shorter than 2000 Å but predicts substantially too much flux at wavelengths from 2000 to 3200 Å. The difference is plausible in view of the probable metallicity differences among these galaxies. Since NGC 3379 and NGC 4472 have closely similar values of Mg_2 (0.329 vs. 0.331 mag), the turnoff population of NGC 3379 is apparently a good match to that in NGC 4472. However, NGC 4649 has Mg_2 stronger by 0.030 mag. It therefore requires a redder turnoff population, but this is not reflected in the NGC 3379-based model. Hence the model turns out to be too blue between 2000 to 3200 Å.

We note that the contributions of V light by the UV components models is small in all cases: 0.5% of CSF and 0.11% of PAGB to convert the SED of NGC 3379 to that of NGC 4472; 3.7% of CSF and 0.9% of PAGB to convert the SED of NGC 3379 to that of NGC 4649.

Since NGC 221 is the elliptical galaxy with the lowest far-UV flux, it is of interest to ask how much V light must be contributed by the PAGB model to reproduce that flux. Figure 7 shows that a V flux of order 0.10%–0.15% from the PAGB $0.565 M_{\odot}$ model yields a satisfactory match.

Finally, Figures 8a and 8b document explicitly the metallicity dependence of the cool stellar component. Figure 8a plots the observed SEDs of NGC 221, NGC 3379, and NGC 4649 in the wavelength region 2200–3200 Å. Using the above models, we can subtract off a model of the hot-UV component to look at the cool stellar component alone. Since the PAGB models contribute the least relative flux in this wavelength region, we have conservatively subtracted the model PAGB $0.565 M_{\odot}$ light distribution from the observed flux for NGC 3379 and NGC 4649. The resulting spectra are plotted in Figure 8b, together with the observed spectrum of NGC 221 (since the UV contamination in this galaxy is so small at these wavelengths).

These three galaxies were chosen as representative of the full range of metallicity in our sample, with NGC 4649 the most metal-rich and NGC 221 the most metal-poor. Figure 8b indicates large differences among the galaxies in the sense expected. The 2600–3000 Å color of metal-rich NGC 4649 averages 0.5 dex (1.25 mag) redder than that of NGC 221, not as large as the (1550 – V) difference, but still much bigger than any visual or IR difference. The UV line strengths in NGC 4649 are about twice as deep as those in NGC 221, which is comparable to the visual absorption-line difference. It is noteworthy that these differences are almost completely masked in the composite spectra of the most metal-rich ellipticals by the presence of the hot UV component (cf. Figs. 2a and 4b). Clearly, age dating of elliptical galaxies via population modeling will have to take the UV component into account. If this can be done, the 2600–3000 Å spectrum may ultimately provide better constraints on age and composition than are available now from ground-based data.

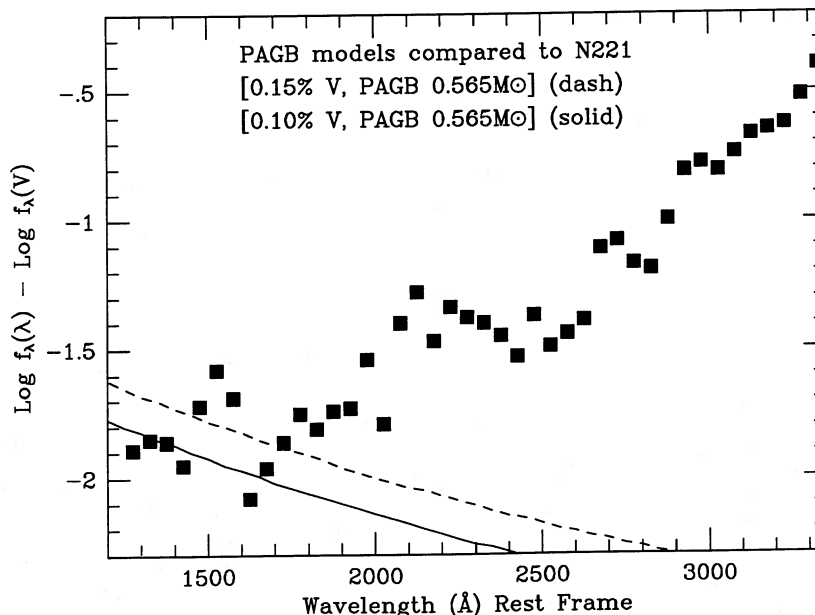


FIG. 7.—An estimate of the amount of PAGB $0.56 M_{\odot}$ model light that would be required to match the far-ultraviolet flux in NGC 221, the quiescent galaxy with the reddest (1550 – V) color.

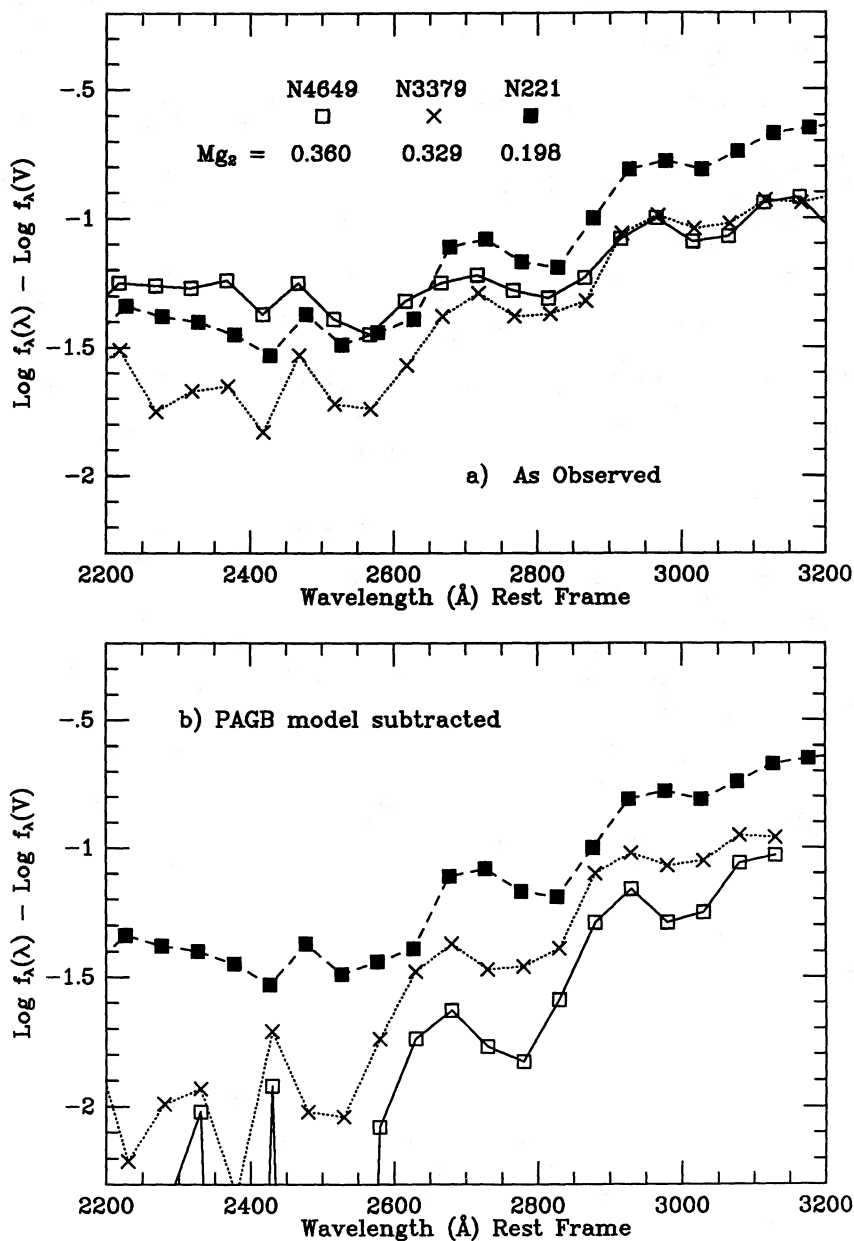


FIG. 8.—(a) The observed SEDs of NGC 221, 3379, and 4649 between 2200 and 3200 Å. (b) The inferred energy distributions for NGC 3379 and NGC 4649 in this wavelength region after a PAGB hot stellar component is subtracted (symbols the same as in [a]). These are compared to the observed energy distribution of NGC 221. The Mg_2 indices for each galaxy are given. The percentage of subtracted V light for the $0.565 M_{\odot}$ PAGB model in NGC 4649 is 0.9% and for NGC 3379, 0.25%. This figure explicitly demonstrates higher line strengths in the underlying stellar population at higher metallicity, an effect that is normally masked by the nonnegligible contribution from the hot component in this wavelength.

V. THE ULTRAVIOLET SPECTRA OF THE "ACTIVE" GALAXIES

Of the four "active" galaxies, the ultraviolet spectrum of N4486 (= M87) has been most discussed (e.g., Bertola *et al.* 1980; Perola and Tarenghi 1980; Nesci and Perola 1985). As noted by Nesci and Perola, previous reductions of the two long-wavelength spectra of NGC 4486 differed substantially in their energy distributions between 2000 and 2600 Å. However, after the present data reductions using IHAP, the three SW and LW revised *IUE* spectra for this galaxy yield consistent energy distributions, within the observed S/N , 0.15–0.3 dex.

The resulting UV energy distributions for NGC 4486 and N6166 are quite similar (see Fig. 2h), but are different from the

quiescent galaxies with similar (1550 – V) colors. As a test of this difference, Figure 9 compares the energy distribution of NGC 4486 to two models which add the Tinsley CSF model and the PAGB model to the energy distribution of NGC 3379. Both are significantly better than the analogous fits to NGC 4649, despite the fact that NGC 4649 and NGC 4486 have similar UV energy distributions shortward of 1800 Å. The fact that NGC 4486 has a bluer SED than NGC 4649 at wavelengths longer than 2400 Å was first noted by Bertola, Capaccioli, and Oke (1982). Furthermore, the predicted level of young star contamination for NGC 4486 is very similar to that predicted for NGC 6166 by Bertola *et al.* (1986).

The lower metallicity of NGC 3379 appears to provide a

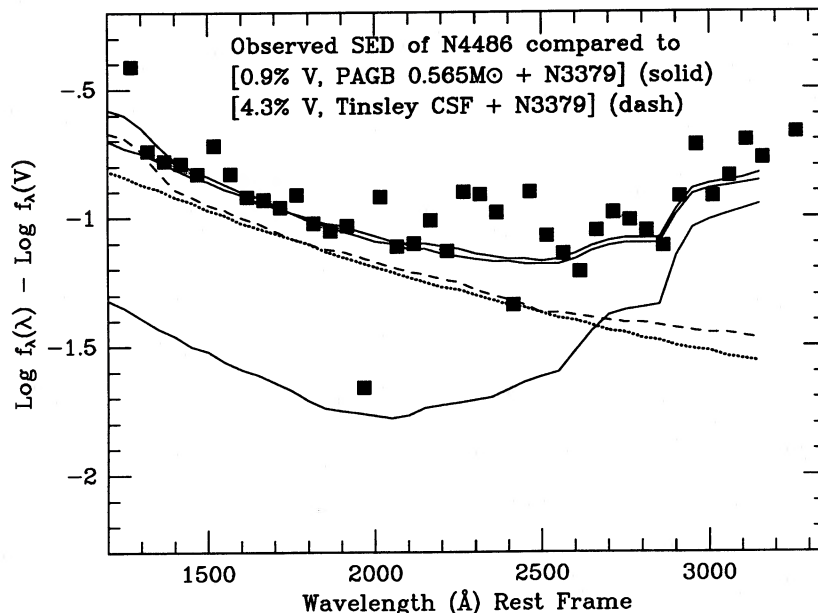


FIG. 9.—Similar to Fig. 6, this time comparing NGC 3379 + model) to the bluest active galaxy, NGC 4486

good match to the energy distribution of NGC 4486 in the range 2500–3200 Å. Whether this is due to a true match in metallicity or to a younger mean turnoff age in NGC 4486 coupled with a higher mean metallicity cannot presently be determined.

Finally, we note the possible presence of slight excess flux relative to the model from 2100 to 2500 Å in NGC 4486 and, by inference also in NGC 6166. This excess was also apparent in Figure 2*h*. As noted in § III*b*, this may indicate an unusual hot stellar population in active galaxies or, alternatively, an extra, nonstellar source of UV radiation.

VI. POSSIBLE ORIGINS FOR THE FAR-UV FLUX

Broadly speaking, there are just two categories of models for the UV flux: young stars and old stars. On the one hand, the observation that many elliptical galaxies contain hot X-ray-emitting gas (Forman, Jones, and Tucker 1985) and that many also have central cooling flows (e.g., Fabian, Nulsen, and Canizares 1982) suggests one kind of young star model, continuing star formation. On the other hand, PAGB and other hot stars are an inevitable product of any old stellar population. Do the UV flux levels and/or the systematic behavior of the flux with metallicity favor either of these alternatives?

a) Continuous Star Formation and Cooling Flow Models

If cooling flows are making stars with a normal initial mass function (IMF), then the (1550 – *V*) magnitude should correlate with the predicted mass infall rate. Silk *et al.* (1986) and Sarazin and O’Connell (1983) have shown that the optical *UBV* colors of elliptical galaxies vary little with respect to the inferred level of star formation injected by a cooling flow. This lack of correlation has led a number of workers to conclude that most of the mass goes into forming very low-mass stars (Fabian, Nulsen, and Canizares 1982). However, Silk *et al.* (1986) show that *UBV* colors are not very sensitive to the IMF and suggest that a normal, solar neighborhood IMF is not ruled out. The far-UV colors should be a more stringent test of ongoing star formation with a normal IMF.

Reliable X-ray fluxes are available for 12 elliptical galaxies in our sample for Forman, Jones, and Tucker (1985) and Thomas *et al.* (1986). The relevant X-ray and UV data are given in Table 4. Distances are calculated on the basis of $H_0 = 50 \text{ km s}^{-1} \text{ kpc}^{-1}$; however, eight galaxies are in the Virgo Cluster and two are in the Fornax cluster. The specific mass infall rate \dot{M} ($M_\odot \text{ yr}^{-1} M_V^{-1} = -22$), is calculated from L_x using equation (14) of Silk *et al.* and scaled to an absolute *V* magnitude of $M_V = -22$. These rates are plotted versus (1550 – *V*) color in Figure 10.

Also shown in Figure 10 is a predicted model relation between gas flow rate and UV color assuming ongoing star formation. The SED of the young population has been taken from models in Figure 6 of Silk *et al.* It is based on a Miller-Scalo IMF with $\text{mass}_{\text{min}} = 0.8 M_\odot$, $\text{mass}_{\text{max}} = 25 M_\odot$, and a uniform rate of star formation. The precise duration of star formation is unimportant as long as it exceeds 1 Gyr, as a steady-state UV flux is quickly reached. Further details are given in the figure legend.

TABLE 4
X-RAY FLUXES AND MASS FLOW RATES

Galaxy (NGC)	M_{G_2}	(1550 – <i>V</i>)	M_V^a	Distance ^a	$\log \dot{M}/M_V^b$ (relative to $M_V = -22$)
1052	0.318	3.06	–21.9	28.7	–0.369
1399	0.357	2.05	–22.5	27.9	0.739
1404	0.344	3.30	–22.1	27.9	0.358
4374	0.323	3.55	–22.4	20.5	–0.585
4382	0.242	4.22	–22.6	20.5	–0.959
4406	0.330	3.72	–22.7	20.5	0.090
4472	0.331	3.42	–23.3	20.5	–0.061
4486	0.303	2.04	–23.1	20.5	0.568
4552	0.346	2.35	–21.9	20.5	–0.482
4649	0.360	2.24	–22.8	20.5	–0.168
4697	0.320	3.41	–21.5	20.5	–1.102
6166	0.324	2.04	–24.2	180.0	1.083

^a $H_0 = 50 \text{ km s}^{-1} \text{ Mpc}^{-1}$.

^b In solar masses per year.

At first glance the model fit seems satisfactory. The absolute level of UV flux seems about right, and there is even a trend in the sense that the galaxies with high flow rates are bluer. However, any theoretical interpretation of such a trend is complicated by the fact that the ratio of X-ray flux to optical luminosity is known to increase proportionally with brighter absolute magnitude ($L_x \propto L_{\text{opt}}^2$; Forman, Jones, and Tucker 1985). Indeed, such a relationship does exist between \dot{M} and M_V for the 12 galaxies given in Table 4. Since a separate relationship is known to exist between M_V and $(1550 - V)$ color (§ III), one expects *a priori* that \dot{M} and $(1550 - V)$ color will be correlated, independent of whether or not there is a direct physical connection between mass cooling flow rates and UV color.

There are also theoretical uncertainties in converting the predictions of global cooling flow models to star formation rates in the centers of these galaxies. The existence of the $(1550 - V)$ - Mg_2 relationship for these galaxies would imply that star formation rates in the centers of cooling flows should be sensitive to metallicity. This in turn implies that the metallicity of the cooling flow would affect both the cooling flow rates and the temperature structure of the hot gas. However, these possibly important details have not yet been incorporated into any cooling flow models.

Although interpretation of Figure 10 is admittedly ambiguous, it is roughly consistent with simple models of star formation due to cooling flows. This is in comparison to the mixed results obtained from comparison with optical colors (cf. Silk *et al.* 1986; and Sarazin and O'Connell 1983). Future observations are proposed in § VII that should yield more direct evidence for ongoing star formation in elliptical galaxies.

b) Old Stellar Populations: Post-Asymptotic Giant Branch Stars

At least three types of hot stars are expected in an old stellar population (Renzini and Buzzoni 1986): accreting white dwarfs, hot horizontal-branch stars, and post-asymptotic giant branch (PAGB) stars (i.e., planetary nebula nuclei). Accreting white dwarfs in binary systems are hard to constrain with known physical models, although their relative level in a stellar population could be a function of metallicity (Greggio and Renzini 1983). Lacking a detailed physical model, we do not consider them further. The number of the hottest horizontal branch stars in Galactic globular clusters are too few relative to the rest of the stellar population to produce the steep blue UV upturn that is seen in the ellipticals. This is true even in clusters with the bluest horizontal branches, which show a flat spectrum from 1500 to 2200 Å as observed with *ANS* (van Albada, de Boer, and Wilkins 1981). We note, however, that ad hoc modifications to the distribution of hot HB stars can produce steep UV upturns (e.g., Nesci and Perola 1985). This leaves PAGB stars as the only plausible hot old stellar component for which a reasonable physical model can currently be constructed.

The PAGB hypothesis is consistent with the apparent lack of bright OB stars in either NGC 221 or NGC 224 (e.g., Bohlin *et al.* 1985), and with the lack of strong absorption lines in the spectra of quiescent early-type luminous galaxies near 1300 Å (§ IIIb). The lack of planetary nebula emission lines is likewise understandable if the core mass of the PAGB stars is lower in ellipticals than in solar neighborhood PAGB stars. Low core masses are needed to match the high levels of UV flux. The

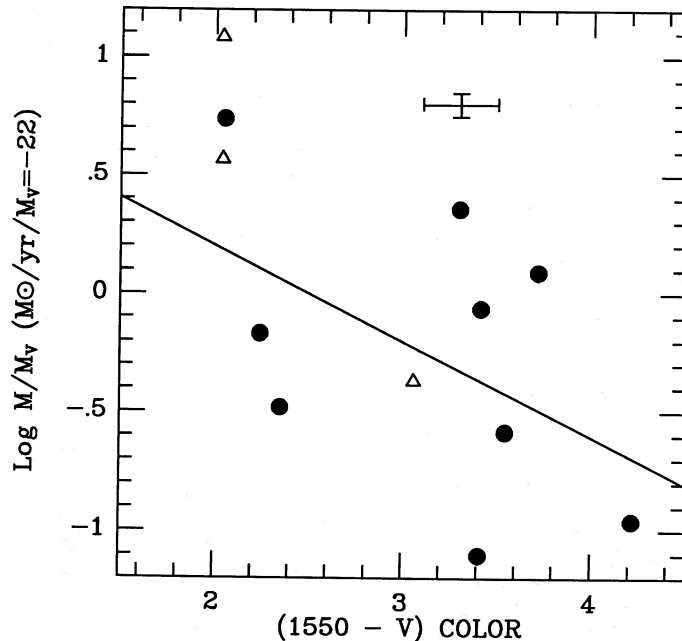


FIG. 10.—X-ray cooling flow rate, \dot{M} , normalized to $M_V = -22$ vs. $(1550 - V)$ color for nine quiescent galaxies (closed circles) and three active galaxies (open triangles) with measured X-ray flux (Table 4). The error bar for \dot{M} is the observational error in L_x alone. The solid line is a model prediction based on the continuing star formation models of Silk *et al.* (1986). Models were calculated for 1, 5, and 17 Gyr, but they all agree closely, so only the 5 Gyr curve is shown. Models use a Miller-Scalo IMF and maximum and minimum stellar masses of $25 M_\odot$ and $0.08 M_\odot$. The contribution of young starlight relative to old is derived on the assumption that $M/L_V(\text{old}) = 6$.

TABLE 5
REQUIRED AND PREDICTED PAGB V FLUXES

Core Mass (M_c)	NGC 221 ^a	NGC 4649 ^a	Model Prediction ^b
0.565 M_\odot	0.14%	0.9%	0.045%
0.545 M_\odot	0.17	1.1	0.25

^a V flux needed to yield observed UV flux, based on the (1550 - V) color.

^b Based on Schoenberner's 1983 evolutionary tracks. See text for details.

lifetimes of low-core mass PAGB stars are so long that the nebula expands and dissipates before the star can heat up and ionize the nebula, unlike the more massive planetary nebula nuclei near the Sun.

The question is not *if*, but *how many* PAGB stars are present in an old stellar population, and whether their integrated flux increases with increasing metallicity in a way that is consistent with Figure 1a. To address the absolute level, we start with NGC 221, whose composition is thought to be comparable to local solar neighborhood stars (Faber 1973), i.e., $[\text{Fe}/\text{H}] \approx -0.2$. The V flux levels of the two PAGB models from Figure 5 are summarized in Table 5, as fitted to NGC 221. These levels can also be predicted from theory, based on the total bolometric luminosity of the PAGB phase and the fuel-consumption theorem of Renzini and Buzzoni (1986). The latter can be used to compare the PAGB total L_{bol} with that of the giant branch, and thus through stellar population models, to the V flux of the galaxy. These predicted fluxes for the two PAGB models are also shown in Table 5. One finds that required levels are 0.14%–0.17% versus predicted levels of 0.05%–0.25%. The agreement is quite reasonable and suggests

a mean PAGB core mass of $M_c = 0.55 \pm 0.01 M_\odot$ in NGC 221, based on Schoenberner's (1983) evolutionary tracks.

Iben and Renzini (1983) offer a formula relating the planetary core mass, M_c , to the initial main-sequence mass, M_i , and the mass-loss rate. This assumes a Reimers (1975a, b) mass-loss rate with free rate parameter η . They note that Galactic globular cluster giant branch tip luminosities imply $\eta = 0.40 \pm 0.04$, with little or no dependence on $[\text{Fe}/\text{H}]$. Using their formula, we find that to fit $M_c = 0.55 M_\odot$ in M32 with $[\text{Fe}/\text{H}] = -0.2$ and age 12.5–15 Gyr requires $\eta = 0.45$ –0.58 (based on stellar isochrone turnoff masses by Vandenberg 1985), which is in tolerably good agreement. An age for NGC 221 as low as 6 Gyr (e.g., O'Connell 1980) would in contrast require $\eta \approx 1.00$.

Although PAGB models match the UV flux level of NGC 221 rather nicely, the *increase* in UV flux with metallicity is harder to explain. The PAGB flux needed to model NGC 4649, a typical high-UV galaxy, is also shown in Table 5. Compared to NGC 221, 7 times as much UV light is needed. This is comparable to the difference in UV output between the two PAGB models, which have core masses that differ by 0.02 M_\odot . Therefore, if NGC 221 planetaries have $M_c = 0.55 M_\odot$, those in NGC 4649 must have $M_c \approx 0.53 M_\odot$, or $\Delta M_c = -0.02 M_\odot$.

According to the Iben-Renzini formula, such a difference could come from smaller initial M_i (down by $\sim 0.12 M_\odot$), from a higher mass-loss rate (up by 60%), or a combination of both. Several ways to produce these by varying age and composition are explored in Table 6 (details given there). None of these models looks attractive. The basic problem is that the higher metallicity of NGC 4649 naturally tends to increase the turnoff

TABLE 6
EFFECT OF EVOLUTIONARY PARAMETERS ON PLANETARY NEBULA CORE MASSES

Model (1)	Change in Main-Sequence Mass M_i (M_\odot) ^a (2)	Change in Core Mass M_c (M_\odot) ^b (3)	Remarks ^c (4)
Change in age, Y or Z :			
Age: from 8 to 12.5 Gyr ^d	-0.12	-0.02 ^e	Right way
Y : from 0.20 to 0.30 ^f	-0.19	-0.03 ^e	Right way
$[\text{He}/\text{H}]$: from 0.0 to 0.5 ^g	+0.16	+0.03 ^e	Wrong way
Change both Y and Z , $\Delta Y = 3\Delta Z$ ^h			
$[\text{Fe}/\text{H}]$: from 0.0 to 0.5; Y : from 0.25 to 0.36	+0.01	+0.00 ^e	No effect
Change in mass-loss rate: ⁱ			
η : from 0.33 to 0.52	-0.02	Right way
Self-consistent Model 1:			
$\Delta Y = 0$; Fixed Y ; Fixed age = 12.5 Gyr; $[\text{Fe}/\text{H}]$: from 0.0 to 0.5;			
$\eta = 0.33$ (no change) ^j	+0.16	+0.03	Wrong way
Self-consistent Model 2:			
$\Delta Y = 3\Delta Z$ ^h ; Fixed age = 12.5 Gyr; Y : from 0.25 to 0.36; $[\text{Fe}/\text{H}]$: from 0.0 to 0.5;			
η : from 0.33 to 0.41 ^j	+0.01	-0.008	Too small

^a M_i is initial main-sequence mass of stars just now making planetaries. It is taken to be the mass of stars at the foot of the giant branch in the isochrones of Vandenberg 1983 and 1985.

^b Core mass as a function of η and M_i is taken from Iben and Renzini 1983, p. 298. No composition dependence is given by these authors, which may be an important omission.

^c A net change in M_i of $-0.02 M_\odot$ is needed to transform NGC 221 into NGC 4649.

^d At $[\text{Fe}/\text{H}] = 0.0$, $Y = 0.25$; Vandenberg 1985.

^e Approximately valid for η in the range 1/3–2/3.

^f At $[\text{Fe}/\text{H}] = 0.0$, $t = 10$ Gyr; Vandenberg 1983.

^g At $Y = 0.25$, $t = 12.5$ Gyr (from extrapolation of Vandenberg 1983 and 1985).

^h At $t = 12.5$ Gyr (from extrapolation of Vandenberg 1983 and 1985). This implies $Y(\text{primordial}) = 0.20$, which is a problem cosmologically.

ⁱ η is a free parameter in Reimers's 1975a, b mass-loss formula (mass loss in proportional to η). For further discussion see Iben and Renzini 1983.

^j The self-consistent models take into account the effect of metallicity on η . This is taken from Reimers's 1975a, b mass-loss formula (as quoted by Iben and Renzini 1983), plus giant-branch isochrones of Ciardullo and Demarque 1977 for different compositions. η is sensitive to composition via its dependence on gravity and luminosity. In Model 1 there is not net change in η , while η increases in Model 2.

mass, not decrease it. This can be partially mitigated by manipulating the helium content in addition to Z and by taking into account the natural dependence of η on L and g , but none of the obvious models quite succeeds. Only making NGC 221 much younger (< 6 Gyr) or arbitrarily upping η in NGC 4649 would have enough leverage to do the job. This would in turn imply a sequence in age and/or η among ellipticals that correlates with metallicity. We do not find either of these options overwhelmingly attractive. Although independent evidence does exist for a younger age for NGC 221 (O'Connell 1980; Burstein *et al.* 1984), as noted above this would require a significantly larger value for η in NGC 221 (~ 1.0) than in Galactic Globular clusters (0.4). Finally, we note the possibility exists that composition might alter the (M_i , η , M_c) relation. Iben and Renzini (1983) hint that M_c goes down as $[\text{Fe}/\text{H}]$ goes up, but gives no quantitative information.

VII. CONCLUSIONS AND FUTURE PROSPECTS

The discovery that the UV flux varies systematically with another physical variable—probably composition—has *not* as of this writing opened the door to a natural explanation for the UV flux in either quiescent or active galaxies. The difficulties with young star and old star, PAGB models lie both with the kind of data currently available (integrated spectral energy distributions) and basic gaps in our current theoretical understanding of star formation and stellar death. Therefore, we conclude that it is still premature to try to choose between these alternatives at this time.

On the other hand, it should be possible very soon to either rule out, or establish, the presence of hot, young main-sequence stars in elliptical galaxies in one of two ways:

1. Such stars should be detected as individual sources of far-UV light in nearby early-type galaxies using the spatial resolution that will be available with the Hubble Space Telescope. Imaging of the center of M31 by Bohlin *et al.* (1985) has already placed an upper limit of B3 or later on the brightest

main-sequence stars that could exist in the M31 bulge. If stars B5 or hotter can be excluded from existing in the bulge of M31, this would effectively rule out hot young stars as the source of far-UV flux in that galaxy.

2. Continuing star formation produces at least 5 times as much flux at visual wavelengths compared to a hypothetical PAGB source and visual light contributions can amount to several percent. The light from a young stellar component will contribute enough flux (2%–5% at visual wavelengths; 4%–10% at shorter optical wavelengths) to be detected in the most metal-rich galaxies. In contrast, PAGB light does not contribute more than 1% of the visual light in any galaxy. Limits of $< 4\%$ hot star contamination at 4000 Å to the old stellar populations of NGCs 4406, 4472, and 3379 have been determined by Rose (1985). However, these limits are still high enough to be compatible with young star models for these particular galaxies. Similar kinds of studies for the most metal-rich galaxies, like NGC 4649, would be very valuable.

We therefore conclude this paper on a hopeful note: With a combined attack using new observations, new telescopes and new theory, the origin of the far-UV flux in early-type galaxies may soon be a solved problem.

We wish to thank Drs. W. G. Mathews, R. F. O'Connell, P. Demarque, A. Renzini, and J. Rose for stimulating discussions. We thank the staff of Villafranca and particularly Drs. W. Wamsteker and A. Cassatella for providing software support and assistance. Mr. M. Fanelli kindly supplied the mean B1.5 V star spectrum in Figure 3, Dr. R. Ellis kindly supplied the LWP spectrum of NGC 4621, and the anonymous referee supplied helpful comments. We gratefully acknowledge the hospitality of UCSC and the University of Padova. This research was supported by NASA/IUE grants NAG5-547 and NAG5-436, in part by an ASU Faculty Grant-in-aid, and in part by NSF grant AST84-20352.

APPENDIX

STAR-FORMING EARLY-TYPE GALAXIES

a) *Blue Vectors for Hot Populations in the Mg_2 -(1550 - V) Diagram*

Considerable evidence has established that young stars can and do form in certain selected early-type galaxies and that the spectra are basically a mixture of an underlying old stellar population and a contaminating, hotter population of younger stars (e.g., NGC 205 [Hodge 1973; Price and Grasdalen 1983] and N5102 [Pritchett 1979]). Burstein (1979) has shown that the blue colors and weak Mg_2 values in NGC 205 and NGC 5102 can be understood in this way. Both color and Mg_2 change with increasing obvious amounts of star formation, moving the measured values of the whole stellar population along a "bluing vector." The slope and length of the bluing vector depend on the color of the star forming population, the percentage of V contamination, and the mean metallicity of the underlying old stars.

The Mg_2 -(1550 - V) diagram lends itself naturally to this kind of analysis: Quiescent galaxies can be thought of as a well-defined "old" stellar population sequence, with both the active and star-forming galaxies lying to the blue of this sequence. Since the effective wavelength of Mg_2 lies within the V passband, the (1550 - V) color of the contaminating blue stellar population by itself is sufficient to determine the slope of the bluing vectors. The length of the vector is determined by the percentage contribution (at either V or 1550 Å) of the contaminating population. Alternatively, if the percentage contribution in V of the star-forming population can be determined by independent means, both the properties of the underlying old stellar population and the (1550 - V) color of that star forming population can be inferred.

This kind of analysis can yield only limited results. It does not assume that the "old" stellar population is *not* forming stars but only that it defines the properties of the normal underlying stellar population in early-type galaxies. Moreover, the (1550 - V) color of the young population determined by this procedure is the net "observed" color, including any extinction effects due to dust. Determination of extinction must come from a more detailed analysis of the whole SED.

b) NGC 5102 and NGC 205

Enough facts are known about the star-forming populations in NGC 5102 and NGC 205 to constrain the $(1550 - V)$ color of their young stars. From the UV spectra alone, one sees by inspection that the energy distributions are relatively flat, varying by no more than 0.1 dex from 1200 Å to 3200 Å, and decreasing by no more than a factor of 2 from the V passband to 1200 Å. Moreover, optical spectra of the regions covered by the *IUE* apertures in these two galaxies show A-type Balmer absorption-line features (S. M. Faber, D. Burstein, *et al.*, unpublished), indicating that the young stellar population contributes substantial flux at V . Thus, a nearly "neutral," or flat, bluing vector is indicated for the contaminating population, in which $\text{flux}_\lambda(1550) = \text{flux}_\lambda(V)$.

The origin of the bluing vector in $[(1550 - V), \text{Mg}_2]$ coordinates can also be inferred from available data. An independent estimate of the metallicity of the stars in N205 has been made by Mould, Kristian, and Da Costa (1984), who give a mean value of $[\text{Fe}/\text{H}] = -0.85 \pm 0.2$ for the old stellar population. From the correlation of Mg_2 with $[\text{Fe}/\text{H}]$ for galactic globular clusters (Burstein *et al.* 1984), this metallicity corresponds to a value of $\text{Mg}_2 = 0.10$, in agreement with our unpublished measurements, after correction for contamination by the young stellar component.

In NGC 5102 an estimate of the metallicity of the underlying old stellar population can be deduced from the outerparts of the galaxy, which have substantially less star formation. The raw $(B - V)$ color is about 0.75 mag (van den Bergh 1976; Pritchet 1979). Allowance for some star formation in the outer regions as well as a metallicity gradient within the galaxy implies that the $(B - V)$ color of the old stellar population at the center is near 0.85 (raw), or 0.80 (reddening-corrected). From Burstein *et al.* (1984), this corresponds to a central Mg_2 value of approximately 0.16. Again, this is in reasonable agreement with the observed Mg_2 after a rough correction for young-star contamination.

These Mg_2 values and their corresponding $(1550 - V)$ colors along the sequence of quiescent galaxies were used as starting points. A series of bluing vectors was then constructed covering a wide range in $(1550 - V)$ color. As expected, a satisfactory match for both NGC 5102 and NGC 205 was obtained only with a "neutral" contaminating energy distribution, in which $f_\lambda(1550) = f_\lambda(V)$, as shown in Figure 11. These vectors predict a 54% contribution to V light by young stars in NGC 5102 and 33% in NGC 205. These estimates are generally consistent with the mixtures of A star and old stellar population absorption lines observed in the spectra near 5000 Å.

c) NGC 2681 and NGC 4742

Although the UV spectra of NGC 2681 and NGC 4742 are significantly redder than NGC 205 and NGC 5102, their optical spectra exhibit relatively strong values of $\text{H}\beta$ compared to Mg_2 : On the absorption line system of Faber *et al.* (1985), $\text{H}\beta$ in the *IUE* aperture ≈ 3.8 Å in NGC 2681, and 3.3 Å for NGC 4742. These values are comparable to the values of 4.5 Å observed for NGC 5102 and 3.7 Å for NGC 205. A-type stars have maximum $\text{H}\beta \approx 6-8$ Å, while old stellar populations with $\text{Mg}_2 = 0.2-0.3$ typically have $\text{H}\beta$ only 2.0-2.4 Å. Thus, the percentage contamination at 4900 Å light by the young population must be at least 33% for NGC 2681 and 20% for NGC 4742. The percent contamination at V will be 10%-20% less (cf. Burstein *et al.* 1984). With this

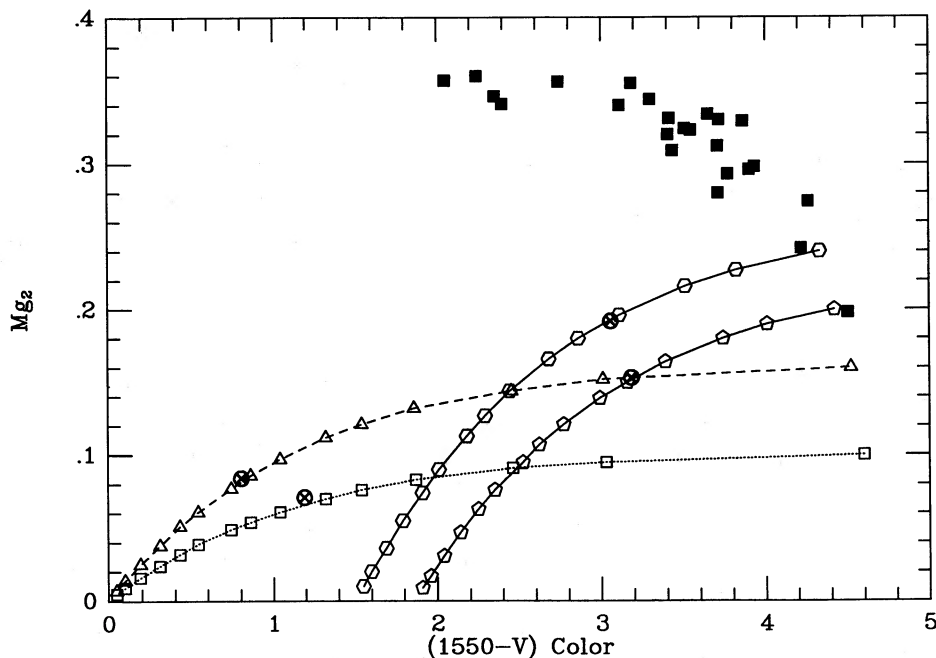


FIG. 11.—(dashed lines, open squares, and triangles): "Bluing vectors" corresponding to a neutral energy distribution [i.e., $f_\lambda(1550) = f_\lambda(V)$], for underlying old stellar populations having Mg_2 values of 0.10 for NGC 205 and 0.16 for NGC 5102. The points plotted along each vector denote 0, 5, 10, 20, 30, 40, 60, 80, 100, 150, 200, 500, 2000% of V light contamination added to the base old stellar population. A V light contamination of about 54% fits the Mg_2 , $(1550 - V)$ parameters of NGC 5102, and a contamination of about 33% fits NGC 205. (solid lines, open hexagons, and pentagons): Bluing vectors corresponding to $f_\lambda(1550) = 0.20f_\lambda(V)$ and a base $\text{Mg}_2 = 0.24$ for NGC 4742 (higher curve) and $f_\lambda(1550) = 0.15f_\lambda(V)$, $\text{Mg}_2 = 0.20$ for NGC 2681 (lower curve). For these two galaxies, the criterion fixing the bluing vector is the percent contamination at V determined by other means: 15% for NGC 4742 and about 25% for NGC 2681. The Mg_2 , $(1550 - V)$ values for the quiescent galaxies (closed squares) are also given for reference, as well as the observed values for the star-forming galaxies (circled Xs).

constraint, it is easy to see from Figure 11 that a "neutral" contaminating energy distribution would contribute far too little at V to produce the observed $H\beta$ line strength for either of these galaxies. The effective contaminating population must be relatively red, perhaps in part due to the effects of internal reddening.

After some experimentation, it became clear that the flux at 1550 \AA should be between 15% and 30% that at V . The resulting bluing vectors are shown in Figure 11 as the solid lines. The vector that intersects the data point for NGC 4742 has a V contamination of 15%, a ratio of $1550/V$ flux of 0.20, and an inferred old stellar population value of $Mg_2 = 0.24$. The bluing vector for NGC 2681 has a V contamination of 25%, $1550/V = 0.15$, and an inferred old stellar population $Mg_2 = 0.20$.

d) "Episodes" of Star Formation in Early-Type Galaxies?

The lack of a strong upturn in the far-UV light in both NGC 5102 and NGC 205 implies that relatively few OB stars are currently being produced. On the other hand, the strong early A-star features in both the *IUE* and the ground ultraviolet (cf. Rocca-Volmerange and Guiderdoni 1987) indicate that major bursts of star formation took place in these galaxies within the age of an A3 star, or about 300 million years ago (e.g., Pritchett 1979). The relatively small number of OB stars necessary to produce the far-UV flux in both galaxies could be the result of residual star formation after this burst.

The redder contaminating stellar populations in NGC 2681 and NGC 4742 are consistent with an epoch of star formation somewhat older than that in NGC 5102—corresponding to main sequence turn-off stars close to F0 in spectral type, with again some residual star formation. This would imply major bursts of star formation in these galaxies 1–2 Gyr ago.

In all four galaxies, the evidence is that most of the star formation occurred during a relatively short period of time—a "burst." The fact that these bursts do not totally dominate the old stellar population makes their integrated stellar populations profitable testing grounds for spectral synthesis mixtures of young and old stars. In turn, understanding such intermediate cases of star formation can be used as a stepping stone toward the more difficult problem of modeling the stellar populations of spiral galaxies.

REFERENCES

- Bertola, F., Capaccioli, M., Holm, A. V., and Oke, J. B. 1980, *Ap. J. (Letters)*, **237**, L65.
 Bertola, F., Capaccioli, M., and Oke, J. B. 1982, *Ap. J.*, **254**, 494.
 Bertola, F., Gregg, M. D., Gunn, J. E., and Oemler, A., Jr. 1986, *Ap. J.*, **303**, 624.
 Bohlin, R. C., Cornett, R. H., Hill, J. K., Hill, R. S., O'Connell, R. W., and Stecher, T. P. 1985, *Ap. J. (Letters)*, **298**, L37.
 Bruzual, G. A. 1983, *Ap. J.*, **273**, 105.
 Burstein, D. 1979, *Ap. J.*, **232**, 74.
 Burstein, D., Davies, R. L., Dressler, A., Faber, S. M., Lynden-Bell, D., Terlevich, R., and Wegner, G. A. 1987, *Ap. J. Suppl.*, **64**, 601 (BDDFLBTW).
 ———. 1988, in *Towards Understanding Galaxies at High Redshift*, ed. R. G. Kron and A. Renzini, in preparation.
 Burstein, D., Faber, S. M., Gaskell, C. M., and Krumm, N. 1984, *Ap. J.*, **287**, 586.
 Burstein, D., and Heiles, C. 1982, *A.J.*, **87**, 1167.
 ———. 1984, *Ap. J. Suppl.*, **54**, 33.
 Burstein, D., Marzke, R., and Condon, M. 1987, in preparation.
 Ciardullo, R., and Demarque, P. 1977, *Trans. Yale Univ. Obs.*, Vol. 33.
 Code, A. D., and Welch, G. A. 1979, *Ap. J.*, **228**, 95.
 Dalle Ore, C. M., Faber, S. M., Burstein, D., and Gonzalez, J. J. 1987, in preparation.
 Davies, R. L., Burstein, D., Dressler, A., Faber, S. M., Lynden-Bell, D., Terlevich, R., and Wegner, G. 1987, *Ap. J. Suppl.*, **64**, 581.
 de Vaucouleurs, G., de Vaucouleurs, A., and Corwin, H. G. 1976, *Second Reference Catalog of Bright Galaxies* (Austin: University of Texas) (RC2).
 Dressler, A. 1980, *Ap. J. (Letters)*, **240**, L11.
 Faber, S. M. 1973, *Astr. Ap. Suppl.*, **10**, 201.
 ———. 1983, *Highlights Astr.*, **6**, 165.
 Faber, S. M., Friel, E. D., Burstein, D., and Gaskell, C. M. 1985, *Ap. J. Suppl.*, **57**, 711.
 Faber, S. M., and Jackson, R. E. 1976, *Ap. J.*, **204**, 668.
 Fabian, A. C., Nulsen, P. E. J., and Canizares, C. R. 1982, *M.N.R.A.S.*, **201**, 933.
 Fanelli, M. N., O'Connell, R. W., and Thuan, T. X. 1987, preprint.
 Forman, W., Jones, C., and Tucker, W. 1985, *Ap. J.*, **293**, 102.
 Fosbury, R. A. E., Snijders, M. A. J., Bokserberg, A., and Penston, M. V. 1981, *M.N.R.A.S.*, **197**, 235.
 Gregg, M. D. 1985, Ph.D. thesis, Yale University.
 Greggio, L., and Renzini, A. 1983, *Astr. Ap.*, **118**, 217.
 Gunn, J. E., Stryker, L. L., and Tinsley, B. M. 1981, *Ap. J.*, **249**, 48.
 Hackney, R. L., Hackney, K. R. H., and Kondo, Y. 1982, in *Advances in Ultraviolet Astronomy: Four Years of IUE Research* (NASA Pub. 2238), p. 335.
 Hodge, P. W. 1973, *Ap. J.*, **182**, 671.
 Holm, A., Bohlin, R. C., Cassatella, A., Ponz, D. P., and Schiffer, F. H. 1982, *Astr. Ap.*, **112**, 341.
- Iben, I., and Renzini, A. 1983, *Ann. Rev. Astr. Ap.*, **21**, 271.
 Johnson, H. R. 1966, *Ann. Rev. Astr. Ap.*, **4**, 191.
 Kjaergaard, P. 1987, *Astr. Ap.*, **176**, 210.
 Lauer, T. R. 1985, *Ap. J. Suppl.*, **57**, 473.
 Lynden-Bell, D., Faber, S. M., Burstein, D., Davies, R. L., Dressler, A., Terlevich, R. J., and Wegner, G. 1988, *Ap. J.*, **326**, 19.
 Malkan, M. A., and Sargent, W. L. W. 1982, *Ap. J.*, **254**, 22.
 Mould, J., Kristian, J., and Da Costa, G. S. 1984, *Ap. J.*, **278**, 575.
 Nesci, R., and Perola, G. C. 1985, *Astr. Ap.*, **145**, 296.
 O'Connell, R. W. 1980, *Ap. J.*, **236**, 430.
 O'Connell, R. W., Thuan, T. X., and Puschell, J. J. 1986, *Ap. J. (Letters)*, **303**, L37.
 Oke, J. B., Bertola, F., and Capaccioli, M. 1981, *Ap. J.*, **243**, 453.
 Perola, G. C., and Tarenghi, M. 1980, *Ap. J.*, **240**, 447.
 Price, J. S., and Grasdalen, G. L. 1983, *Ap. J.*, **275**, 559.
 Pritchett, C. 1979, *Ap. J.*, **231**, 354.
 Reimers, D. 1975a, *Mem. Soc. Roy. Sci. Liège*, 6, Ser. 8, p. 369.
 ———. 1975b, in *Problems in Stellar Atmospheres and Envelopes*, ed. B. Baschek, W. H. Kegel, and G. Traving (Springer: Berlin), p. 229.
 Renzini, A., and Buzzoni, A. 1986, in *Spectral Evolution of Galaxies*, ed. C. Chiosi and A. Renzini (Dordrecht: Reidel), in press.
 Rocca-Volmerange, B., and Guiderdoni, B. 1987, *Astr. Ap.*, **175**, 15.
 Rose, J. A. 1985, *A.J.*, **90**, 1927.
 Seaton, M. J. 1979, *M.N.R.A.S.*, **187**, 73P.
 Sarazin, C. L., and O'Connell, R. W. 1983, *Ap. J.*, **268**, 552.
 Savage, B. D., and de Boer, K. S. 1981, *Ap. J.*, **243**, 460.
 Savage, B. D., and Mathis, T. S. 1979, *Ann. Rev. Astr. Ap.*, **17**, 73.
 Schoenberner, D. 1983, *Ap. J.*, **272**, 708.
 Silk, J., Djorgovski, S. G., Wyse, R. F. G., and Bruzual, G. A. 1986, *Ap. J.*, **307**, 415.
 Thomas, P. A., Fabian, A. C., Arnaud, K. A., Forman, W., and Jones, C. 1986, *M.N.R.A.S.*, **222**, 655.
 van Albada, T. S., de Boer, K. S., and Dickens, R. J. 1981, *M.N.R.A.S.*, **195**, 591.
 VandenBerg, D. A. 1983, *Ap. J. Suppl.*, **51**, 29.
 ———. 1985, *Ap. J. Suppl.*, **58**, 711.
 van den Bergh, S. 1976, *A.J.*, **81**, 795.
 Welch, G. A. 1982, *Ap. J.*, **259**, 77.
 Wu, C.-C., Faber, S. M., Gallagher, J. S., Peck, M., and Tinsley, B. M. 1980, *Ap. J.*, **237**, 290.
 Wu, C.-C., et al. 1983, *The IUE Ultraviolet Spectral Atlas (IUE/NASA Newsletter, No. 22)*.
 Young, P. J., Westphal, J. A., Kristian, J., Wilson, C. P., and Landauer, F. P. 1978, *Ap. J.*, **221**, 712.

F. BERTOLA: Department of Astronomy, University of Padova, 35100 Padova, Italy

DAVID BURSTEIN: Department of Physics, Arizona State University, Tempe, AZ 85287

L. M. BUSON: Astronomical Observatory, 35100 Padova, Italy

S. M. FABER: Lick Observatory, University of California, Santa Cruz, CA 95064

TOD R. LAUER: Princeton University Observatory, Princeton, NJ 08544